



## Urban inland wintertime $\text{N}_2\text{O}_5$ and $\text{ClNO}_2$ influenced by snow-covered ground, air turbulence, and precipitation

Kathryn D. Kulju<sup>1</sup>, Stephen M. McNamara<sup>1</sup>, Qianjie Chen<sup>1†</sup>, Jacinta Edebeli<sup>1,2</sup>, Jose D. Fuentes<sup>3</sup>, Steven  
5 B. Bertman<sup>4</sup>, Kerri A. Pratt<sup>1,5\*</sup>

<sup>1</sup>Department of Chemistry, University of Michigan, Ann Arbor, MI 48109, USA

<sup>2</sup>Paul Scherrer Institut, 5232 Villigen, Switzerland

<sup>3</sup>Department of Meteorology and Atmospheric Science, Pennsylvania State University, University Park,  
Pennsylvania 16802, USA

10 <sup>4</sup>Institute of the Environment and Sustainability, Western Michigan University, Kalamazoo, Michigan  
49008, USA

<sup>5</sup>Department of Earth and Environmental Sciences, University of Michigan, Ann Arbor, MI 48109, USA

<sup>†</sup>Current: Department of Civil and Environmental Engineering, The Hong Kong Polytechnic University,  
Hong Kong SAR, China

15 *Correspondence to:* Kerri A. Pratt (prattka@umich.edu)

**Abstract.** The atmospheric multiphase reaction of dinitrogen pentoxide ( $\text{N}_2\text{O}_5$ ) with chloride-containing  
aerosol particles produces nitryl chloride ( $\text{ClNO}_2$ ), which has been observed across the globe. The  
photolysis of  $\text{ClNO}_2$  produces chlorine radicals and nitrogen dioxide ( $\text{NO}_2$ ), which alter pollutant fates  
and air quality. However, the effects of local meteorology on near-surface  $\text{ClNO}_2$  production are not yet  
20 well understood, as most observational and modeling studies focus on periods of clear conditions. During  
a field campaign in Kalamazoo, Michigan from January-February 2018,  $\text{N}_2\text{O}_5$  and  $\text{ClNO}_2$  were measured  
using chemical ionization mass spectrometry, with simultaneous measurements of atmospheric  
particulate matter and meteorological parameters. We examine the impacts of atmospheric turbulence,  
precipitation (snow, rain) and fog, and ground cover (snow-covered and bare ground) on the abundances  
25 of  $\text{ClNO}_2$  and  $\text{N}_2\text{O}_5$ .  $\text{N}_2\text{O}_5$  mole ratios were lowest during periods of lower turbulence and were not



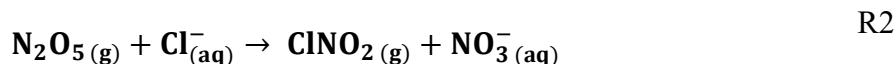
statistically significantly different between snow-covered and bare ground. In contrast, ClNO<sub>2</sub> mole ratios were highest, on average, over snow-covered ground, due to saline snowpack ClNO<sub>2</sub> production. Both N<sub>2</sub>O<sub>5</sub> and ClNO<sub>2</sub> mole ratios were lowest, on average, during rainfall and fog because of scavenging, with N<sub>2</sub>O<sub>5</sub> scavenging by fog droplets likely contributing to observed increased particulate nitrate concentrations. These observations, specifically those during active precipitation and with snow-covered ground, highlight important processes, including N<sub>2</sub>O<sub>5</sub> and ClNO<sub>2</sub> wet scavenging, fog nitrate production, and snowpack ClNO<sub>2</sub> production, that govern the variability in observed atmospheric chlorine and nitrogen chemistry and are missed when considering only clear conditions.

## 1 Introduction

Atmospheric halogen radicals are highly oxidizing agents of tropospheric pollutants (Simpson et al., 2015). Following nighttime formation, the photolysis of nitryl chloride (ClNO<sub>2</sub>) upon sunrise is a source of chlorine radicals (**R1**) at a time when other oxidants, including the hydroxyl radical (OH), are less abundant (Young et al., 2014), leading to enhanced oxidation of volatile organic compounds (Osthoff et al., 2008). ClNO<sub>2</sub> photolysis also releases NO<sub>2</sub> (**R1**), thus recycling nitrogen oxides (NO<sub>x</sub>) that drive ozone formation (Crutzen, 1979).



ClNO<sub>2</sub> is formed by the multiphase reaction of dinitrogen pentoxide (N<sub>2</sub>O<sub>5</sub>) on a chloride-containing surface (**R2**), particularly sea spray aerosol (Finlayson-Pitts and Pitts, 1989; Osthoff et al., 2008).



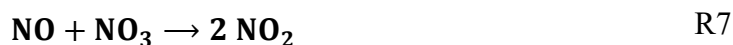
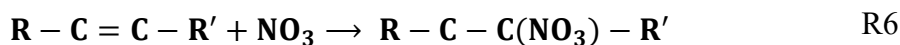
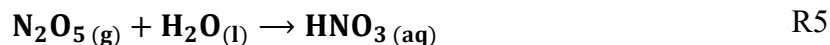
In the Northern Hemisphere, surface-level ClNO<sub>2</sub> abundance is simulated to be highest during winter; this is thought to be due to greater N<sub>2</sub>O<sub>5</sub> abundances, shallower mixed layer heights or even stable boundary layers, lower air temperatures, and higher ClNO<sub>2</sub> yields (Sarwar et al., 2014). ClNO<sub>2</sub> production has been previously studied in the laboratory following the reaction of N<sub>2</sub>O<sub>5</sub> with aqueous aerosols (e.g.



Behnke et al., 1997; Bertram and Thornton, 2009; Roberts et al., 2009; Thornton and Abbatt, 2005) and frozen solutions (Lopez-Hilfiker et al., 2012). A recent modeling study suggests that ClNO<sub>2</sub> may be produced from heterogeneous reaction on the snowpack, in addition to aerosols (Wang et al., 2020). In addition to marine and coastal environments, ClNO<sub>2</sub> has been measured in inland environments, including Boulder, Colorado, USA (Riedel et al., 2013; Thornton et al., 2010), , Calgary, Alberta, Canada (Mielke et al., 2011), Frankfurt, Germany (Phillips et al., 2012), Ji'nan, Shandong, China (e.g. Wang et al., 2017), and southwest of Baoding, Hebei, China (e.g. Tham et al., 2018); in these inland environments, ClNO<sub>2</sub> abundance is typically hundreds of ppt. Recently, a study in Ann Arbor, Michigan identified road salt aerosol as the dominant aerosol chloride source for ClNO<sub>2</sub> production during winter (McNamara et al., 2020). Measurements in Kalamazoo, Michigan also identified the road salt-contaminated snowpack as a ClNO<sub>2</sub> source (McNamara et al., 2021). A study in coastal British Columbia, Canada suggested scavenging of ClNO<sub>2</sub> by rain and/or fog droplets as a potential loss process (Osthoff et al., 2018). However, the authors pointed out that scavenging of the nitrate radical (NO<sub>3</sub>), N<sub>2</sub>O<sub>5</sub>, and ClNO<sub>2</sub> have not been constrained by laboratory investigations (in contrast to other gases like sulfur dioxide (SO<sub>2</sub>) and ammonia (NH<sub>3</sub>)) and so periods of precipitation were excluded from subsequent calculations of N<sub>2</sub>O<sub>5</sub> uptake and ClNO<sub>2</sub> yield (Osthoff et al., 2018).

N<sub>2</sub>O<sub>5</sub>, the precursor to ClNO<sub>2</sub>, is formed from the reaction of NO<sub>2</sub> with NO<sub>3</sub> (**R3**), which is formed from the reaction of NO<sub>2</sub> with ozone (O<sub>3</sub>, **R4**). The formation of N<sub>2</sub>O<sub>5</sub> from NO<sub>2</sub> and NO<sub>3</sub> is a temperature-dependent equilibrium, with N<sub>2</sub>O<sub>5</sub> production favored at lower temperatures (Asaf et al., 2010; Wagner et al., 2013). At a NO<sub>2</sub> background level of 1 ppb, the ratio of N<sub>2</sub>O<sub>5</sub>:NO<sub>3</sub> (**R3**) is ~1 at 295 K, but this N<sub>2</sub>O<sub>5</sub>:NO<sub>3</sub> ratio is ~10 at 278 K (Chang et al., 2011). Loss of N<sub>2</sub>O<sub>5</sub> is an important terminal sink for nitrogen oxides (NO<sub>x</sub> = NO + NO<sub>2</sub>) in the troposphere (Simpson et al., 2015). Long-term data show that direct N<sub>2</sub>O<sub>5</sub> loss via hydrolysis, to produce nitric acid (HNO<sub>3</sub>, **R5**), is most important during winter, and indirect N<sub>2</sub>O<sub>5</sub> loss (removal of NO<sub>3</sub> via reaction with hydrocarbons and NO, **R6-R7**) is most important during summer (Allan et al., 1999; Geyer et al., 2001; Heintz et al., 1996).





Experimental investigations of the impacts of meteorology on  $\text{N}_2\text{O}_5$  abundance are primarily limited to observations of uptake by fog in coastal regions (Brown et al., 2016; Osthoff et al., 2006; 75 Sommariva et al., 2009; Wood et al., 2005). In addition to forming  $\text{HNO}_3$ , hydrolysis of  $\text{N}_2\text{O}_5$  can produce particle-phase nitrate ( $\text{NO}_3^-$ ) (Brown et al., 2004; Osthoff et al., 2006). Particle-phase nitrate has been observed to increase, then subsequently decrease, during fog episodes, which is hypothesized to be the result of  $\text{N}_2\text{O}_5$  hydrolysis to form nitrate, followed by wet removal of nitrate from the fog layer (Lillis et al., 1999).

80 The review by Chang et al. (2011) stated that future observation-based research is need to further investigate how  $\text{N}_2\text{O}_5$  is affected by meteorological conditions, due to its impacts on  $\text{ClNO}_2$  and particulate matter abundances, as well as the oxidative capacity of the atmosphere. Many gaps remain in our understanding of the fates and production of  $\text{N}_2\text{O}_5$  and  $\text{ClNO}_2$ , especially in inland locations, and how they are influenced by meteorological conditions such as precipitation events, fog, and turbulent mixing. 85 Notably, Stanier et al. (2012) identified the impacts of fog and snow cover as important knowledge gaps in understanding wintertime atmospheric composition, and nitrate formation in particular, in the Midwest United States.

The SNow and Atmospheric Chemistry in Kalamazoo (SNACK) field campaign was conducted during January and February 2018 in Kalamazoo, MI on the campus of Western Michigan University 90 (WMU). In our previous publication from this study, we showed photochemical snowpack HONO production due to snow nitrate photolysis (Chen et al., 2019). Through vertical gradient measurements on select nights of the SNACK field campaign, we showed that  $\text{N}_2\text{O}_5$  deposits at the same rates over bare and snow-covered ground; whereas, while  $\text{ClNO}_2$  deposits on bare ground, it can be emitted from the saline snow-covered ground, with snow chamber experiments confirming saline snow  $\text{ClNO}_2$  production 95 (McNamara et al., 2021). Here, we focus on the observational time series of near-surface  $\text{ClNO}_2$  and its precursor  $\text{N}_2\text{O}_5$  and examine the influences of precipitation (rain, snow) and fog, atmospheric turbulence,



ground cover (snow-covered vs bare ground), particulate chloride and nitrate, temperature, and relative humidity (RH) on the night-time abundances of these compounds, measured by chemical ionization mass spectrometry. This study provides new insights into the biases associated with modeling and observations  
100 focused on cloudless (clear) conditions, which has been shown to impact predictions of aerosol chemical composition (Christiansen et al., 2020).

## 2 Methods

The sampling site (42.28°N, 85.61°W) on the campus of WMU in Kalamazoo, MI was located next to a field and was approximately 90 m from a major roadway, as previously described by McNamara  
105 et al. (2020a). As described below, measurements of trace gases (N<sub>2</sub>O<sub>5</sub> and ClNO<sub>2</sub>), PM<sub>2.5</sub> (particulate matter with a diameter ≤2.5 μm) inorganic chemical composition, three-dimensional wind speed, and temperature were conducted at the field site from January 20 to February 24, 2018. Daily photographs and field notes were used to determine ground cover and spatial extent of snow cover.

### 2.1 Meteorological measurements

110 Air temperature and three-dimensional wind speed (*u*, *v*, and *w*) were measured from a height of 1.4 m and at a frequency of 20 Hz using a sonic anemometer (model CSAT3, Campbell Scientific Inc., Logan, UT). The sonic anemometer was not operational from February 20-21 due to complications associated with heavy rainfall. Friction velocity (*u*<sup>\*</sup>) was calculated from turbulent covariance of three-dimensional wind speed based on 30 minute averaging, where *u*' , *v*' , and *w*' are fluctuations about the 30  
115 min mean wind speed in its zonal (*u*), meridional (*v*), and vertical (*w*) components, respectively (E1) (Stull, 1988).

$$u^* = (\overline{u'w'^2} + \overline{v'w'^2})^{\frac{1}{4}} \quad \text{E1}$$

Kinematic heat flux (*w*'*T*') was also calculated from sonic anemometer data, where *w*' and *T*' are deviations in vertical velocity and temperature from five-minute averages, respectively (Monin and Obukhov, 1954). Kinematic heat flux values were then further averaged to obtain 30 min time resolution  
120 quantities. This heat flux value describes the transport of thermal energy by eddies; negative values of



w'T' indicate heat transport from the atmosphere to the surface and are associated with a temperature inversion (Stull, 1988).

Weather conditions (rain, snow, and fog) were recorded at the Kalamazoo–Battle Creek International Airport (KAZO), which was located ~7 km to the southeast; data were retrieved from  
125 Weather Underground (<https://www.wunderground.com/history/daily/us/mi/kalamazoo/KAZO>). Wind speed and temperature data were also obtained from this weather station to supplement the rain case study (February 20-21), during which data from the sonic anemometer were unavailable.

## 2.2 N<sub>2</sub>O<sub>5</sub> and ClNO<sub>2</sub> measurements using chemical ionization mass spectrometry (CIMS)

Measurements of N<sub>2</sub>O<sub>5</sub> and ClNO<sub>2</sub> were conducted using a chemical ionization mass  
130 spectrometer (CIMS, THS Instruments) (Liao et al., 2011). The CIMS instrument uses iodide-water reagent ion clusters, I(H<sub>2</sub>O)<sup>-</sup>, to ionize analyte molecules, which are separated and quantified using a quadrupole mass analyzer. The CIMS was housed in a mobile laboratory trailer at the field site, and sampled ambient air at ~300 L min<sup>-1</sup> through a specialized inlet, designed to prevent wall losses of reactive species (Huey et al., 2004; Neuman et al., 2002), as in previous campaigns (e.g., McNamara et al., 2019).  
135 The inlet consisted of a 30 cm long, 4.6 cm i.d. aluminum pipe attached to a stainless-steel ring torus 1.5 m above ground level. The airflow from this inlet was subsampled at 6.6 L min<sup>-1</sup> into a 48 cm long, 0.95 cm i.d. FEP Teflon tube and through a custom three-way heated valve (30°C) used to obtain calibration and background measurements. Of this airflow, an ozone monitor (model 205, 2B Technologies, Boulder, CO) sub-sampled 1.7 L min<sup>-1</sup>, and 0.9 L min<sup>-1</sup> was sub-sampled into the CIMS ion-molecule reaction  
140 region, which was held at a constant pressure of 15.5 Torr. I(H<sub>2</sub>O)<sup>-</sup> reagent ions (Slusher et al., 2004) were generated by passing iodomethane (CH<sub>3</sub>I) in nitrogen (N<sub>2</sub>) through a <sup>210</sup>Po radioactive ion source. The ion-molecule reaction region was humidified using water vapor from an impinger to prevent changes in ambient RH from altering CIMS sensitivity (Kercher et al., 2009; McNamara et al., 2019).

N<sub>2</sub>O<sub>5</sub> was monitored at *m/z* 235 (IN<sub>2</sub>O<sub>5</sub><sup>-</sup>), and ClNO<sub>2</sub> was monitored at *m/z* 208 (I<sup>35</sup>ClNO<sub>2</sub><sup>-</sup>) and  
145 *m/z* 210 (I<sup>37</sup>ClNO<sub>2</sub><sup>-</sup>), each with dwell times of 1.5 s. ClNO<sub>2</sub> was positively identified using its measured isotopic ratio (**Fig. S1**). Background measurements were conducted for 2 min every 15 min by passing the ambient air flow through a scrubber containing glass wool and stainless-steel wool (heated to 120°C)



(McNamara et al., 2020), which removed  $\text{N}_2\text{O}_5$  and  $\text{ClNO}_2$  with  $96.4\pm 0.8\%$  and  $89\pm 1\%$  efficiency (mean $\pm 95\%$  confidence interval), respectively (McNamara et al., 2021). Calibrations in the field were  
150 conducted every 2 h by adding  $0.2 \text{ L min}^{-1}$  of  $12.3\pm 0.2 \text{ ppb Cl}_2$  (in  $\text{N}_2$ ) from a permeation source (VICI  
Metronics, Inc., Poulsbo, WA) to the ambient airflow. The permeation rate was measured by bubbling  
the permeation output into a solution of potassium iodide and measuring the oxidation product, triiodide  
( $\text{I}_3^-$ ), using UV-visible spectrophotometry at 352 nm (Liao et al., 2011).  $\text{N}_2\text{O}_5$  and  $\text{ClNO}_2$  were calibrated  
offline relative to  $\text{Cl}_2$  as described in McNamara et al. (2019b). The  $3\sigma$  limits of detection (LOD),  
155 corresponding to 2 min background periods, were 1.3 ppt and 0.4 ppt for  $\text{N}_2\text{O}_5$  and  $\text{ClNO}_2$ , respectively.  
We report mole ratios as 30 min averages, for which the  $3\sigma$  LODs for  $\text{N}_2\text{O}_5$  and  $\text{ClNO}_2$  are estimated to  
be 0.3 ppt and 0.1 ppt for  $\text{N}_2\text{O}_5$  and  $\text{ClNO}_2$ , respectively, calculated in the same manner as Liao et al.  
(2011). CIMS measurement uncertainties, which include propagated uncertainties associated with  
calibrations and fluctuations in the background signal, are estimated as  $22\%+0.3 \text{ ppt}$  and  $22\%+0.1 \text{ ppt}$  for  
160 30 min averaged  $\text{N}_2\text{O}_5$  and  $\text{ClNO}_2$  mole ratios, respectively. Because  $\text{N}_2\text{O}_5$  and  $\text{ClNO}_2$  were present  
almost exclusively at night, we define “nocturnal”/“nighttime” as the period between 18:00 and 8:00  
Eastern Standard Time (EST, Coordinated Universal Time (UTC)-5 h), which was approximately  $\pm 30$   
min from sunrise and sunset during the campaign.

$\text{Cl}_2$  was monitored as  $\text{I}(\text{Cl}_2)^-$  at  $m/z$  197 and 199, each with dwell times of 0.5 s. The LOD for  $\text{Cl}_2$   
165 at  $m/z$  197 was 2.4 ppt (0.6 ppt for 30 min averaged data).  $\text{Cl}_2$  was below its estimated LOD for 30 min  
averaging for 96% of the nighttime periods (and 91% of daytime periods), and therefore these limited  
data are not discussed.  $\text{HNO}_3$  was also monitored as  $\text{I}(\text{HNO}_3)^-$  at  $m/z$  190 with a dwell time of 0.5 s and  
calibrated offline relative to  $\text{Cl}_2$  (McNamara et al., 2020). However, there was a high background signal  
due to poor scrubbing efficiency ( $12\pm 1\%$ ), resulting in a high LOD of 43 ppt (11 ppt for 30 min averaged  
170 data). 40% of the nighttime  $\text{HNO}_3$  data during the campaign were below the LOD estimated for 30 min  
averaging, and therefore these data are not discussed quantitatively in this work.

Gas-phase scavenging coefficients ( $\Lambda_g$ ) were calculated for  $\text{N}_2\text{O}_5$  and  $\text{ClNO}_2$  using the method of  
Pruppacher and Klett (1997), where  $c_g^0$  refers to the initial concentration, and  $\frac{dc_g}{dt}$  refers to the change in  
concentration over time:



$$\Lambda_g = \frac{-1}{c_g^0} \times \frac{dc_g}{dt} \quad \text{E2}$$

### 175 **2.3 Ambient ion monitor-ion chromatography (AIM-IC)**

PM<sub>2.5</sub> chloride (Cl<sup>-</sup>) and nitrate (NO<sub>3</sub><sup>-</sup>) were measured by an ambient ion monitor-ion chromatography instrument (AIM-IC; model 9000D, URG Corp., Chapel Hill, NC), as described in Chen et al. (2019). The AIM-IC and custom outdoor sampling inlet is described in detail by Markovic et al. (2012). Briefly, ambient air was sampled at 3 L min<sup>-1</sup> through a 2.5 μm cyclone at a height of 1.8 m. A parallel-plate wet denuder (PPWD) supplied with diluted H<sub>2</sub>O<sub>2</sub> separated soluble inorganic trace gases. Particles entered a supersaturation chamber (SSC), where hygroscopic growth was initiated prior to an inertial particle separator. The PPWD and SSC were placed outside in an insulated and heated aluminum case to reduce the sampling line length. Trace gas and particle samples were collected every hour using on concentrator columns (anion, UTAC-ULP1, ultra-trace anion concentrator ultralow pressure; cation, 185 TCC-ULP1, trace cation concentrator ultralow pressure; Thermo Fisher Scientific, Waltham, MA) for measurements every 2-4 h (3 h after January 24) by an ion chromatograph (ICS-2100; Dionex Inc., Sunnyvale, CA). LiF was used as an internal standard. The 3σ LODs for Cl<sup>-</sup> and NO<sub>3</sub><sup>-</sup> were 0.004 and 0.05 μg m<sup>-3</sup>, respectively, for 3 h sampling.

### **2.4 Aerosol size distribution measurements**

190 Aerosol size distributions were measured using a scanning mobility particle sizer (SMPS, model 3082, TSI, Inc., Shoreview, MN), which measured electrical mobility diameter from 14.1-736.5 nm, and an aerodynamic particle sizer (APS, model 3321, TSI, Inc., Shoreview, MN), which measured aerodynamic diameter from 0.5-20 μm. The air was sampled through a 2.5 μm cyclone (URG Corp., Chapel Hill, NC) from an inlet height of ~3 m. This flow was split from a manifold with a total flow rate of 16.8 L min<sup>-1</sup>

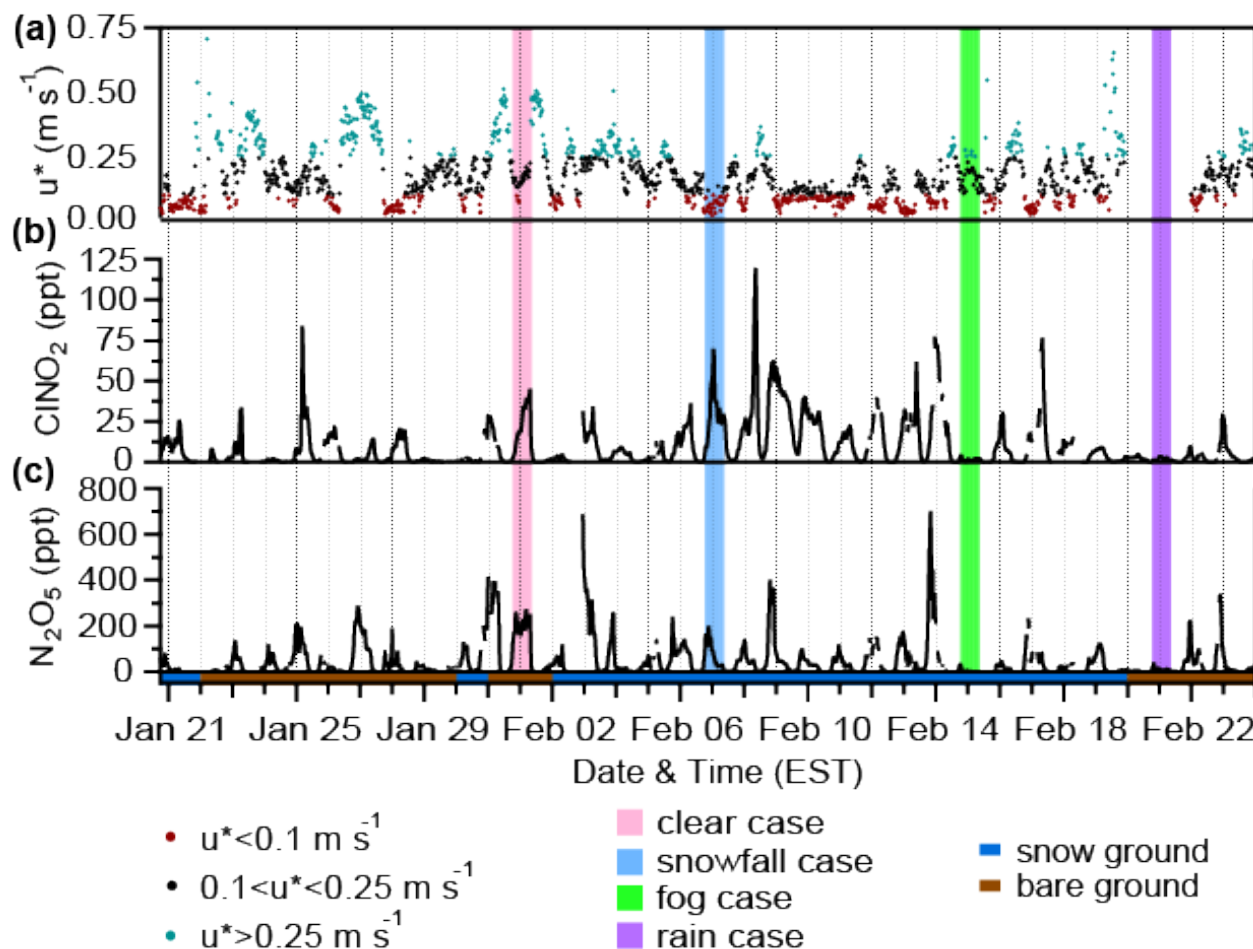




195 into foam-insulated copper tubing for each instrument; the SMPS and APS sub-sampled at  $0.3 \text{ L min}^{-1}$   
and  $4.9 \text{ L min}^{-1}$ , respectively.

### 3 Results and Discussion

The field campaign nights from January 20-February 24 were divided into categories to  
200 investigate the impacts of weather events (rain, snowfall, fog), ground cover (snow-covered and bare  
ground), and atmospheric turbulence on the near-surface ( $\sim 1.5 \text{ m}$  above ground) abundances of  $\text{N}_2\text{O}_5$  and  
 $\text{ClNO}_2$  (**Fig. 1**). Time periods that were below LOD ( $0.3 \text{ ppt}$  and  $0.1 \text{ ppt}$  for 30 min averaged  $\text{N}_2\text{O}_5$  and  
 $\text{ClNO}_2$ , respectively) are included in calculations as  $0.5 \times \text{LOD}$ . Data after 08:00 (approximately  $\pm 30 \text{ min}$   
205 from sunrise, which was at 08:07 on Jan 20 and 07:25 on Feb 24) are not included such that air entrainment  
from the residual boundary layer, discussed elsewhere (e.g. Tham et al., 2016), does not influence the  
results discussed below.



210 **Figure 1:** 30 min averaged (a) friction velocities ( $u^*$ ,  $\text{m s}^{-1}$ ) and (b)  $\text{ClNO}_2$  and (c)  $\text{N}_2\text{O}_5$  mole ratios from January 20 to February 24, 2018. Friction velocities are divided into three categories: lower ( $u^* < 0.1 \text{ m s}^{-1}$ ), intermediate ( $0.1 < u^* < 0.25 \text{ m s}^{-1}$ ), and higher ( $u^* > 0.25 \text{ m s}^{-1}$ ). The shading below the x-axis represents ground cover – snow (blue) or bare ground (brown). Vertical shading represents the example case studies: clear (pink), snowfall (light blue), fog (green), and rain (purple). Gaps in the  $\text{ClNO}_2$  and  $\text{N}_2\text{O}_5$  timeseries are due to experiments described by (McNamara et al., 2021).



### 3.1 Effects of rain, snow, and fog

215 The nighttime abundances of  $\text{N}_2\text{O}_5$  and  $\text{ClNO}_2$  during rain, snowfall, and fog were all significantly  
different ( $p < 0.05$ , t-test) from clear conditions (**Fig. 2**). Average mole ratios for nighttime  $\text{N}_2\text{O}_5$  and  
 $\text{ClNO}_2$  during clear conditions and each type of weather event are listed in **Table 1**, with additional data  
provided in **Table S1**. The average nighttime  $\text{N}_2\text{O}_5$  mole ratios ( $\pm 95\%$  confidence interval) were  $84 \pm 5$   
ppt,  $47 \pm 2$  ppt,  $14 \pm 2$  ppt, and  $7.1 \pm 0.6$  ppt during clear, snowfall, rain, and fog conditions, respectively  
220 (**Fig. 2**). In comparison to clear conditions, average  $\text{N}_2\text{O}_5$  mole ratios were  $37 \pm 5$  ppt (1.8 times),  $70 \pm 5$  ppt  
(6.0 times), and  $77 \pm 5$  ppt (12 times) lower during snowfall, rain, and fog, respectively. The decrease in  
 $\text{N}_2\text{O}_5$  abundance during fog suggests  $\text{N}_2\text{O}_5$  uptake by fog droplets, and is consistent with previous  
observations (Brown et al., 2016; Osthoff et al., 2006; Sommariva et al., 2009; Wood et al., 2005). More  
recently, a study by Osthoff et al. (2018) noted decreased  $\text{ClNO}_2$  abundance during drizzle/rain and fog  
225 during Jul.-Aug. in coastal British Columbia. However, clear conditions are generally the focus of  
previous  $\text{N}_2\text{O}_5$  and  $\text{ClNO}_2$  studies (Chang et al., 2011; Simpson et al., 2015).

**Table 1:** Mean ( $\pm 95\%$  confidence interval) mole ratios of  $\text{N}_2\text{O}_5$  and  $\text{ClNO}_2$  during each type of weather event (clear, snow, fog, and rain) measured across the entire campaign, between 18:00-08:00 EST.

Condition	$\text{N}_2\text{O}_5$ (ppt)	$\text{ClNO}_2$ (ppt)
Clear	$84 \pm 5$	$11.8 \pm 0.7$
Snowfall	$47 \pm 2$	$16.8 \pm 0.7$
Fog	$7.1 \pm 0.6$	$5.0 \pm 0.6$
Rain	$14 \pm 2$	$2.27 \pm 0.06$

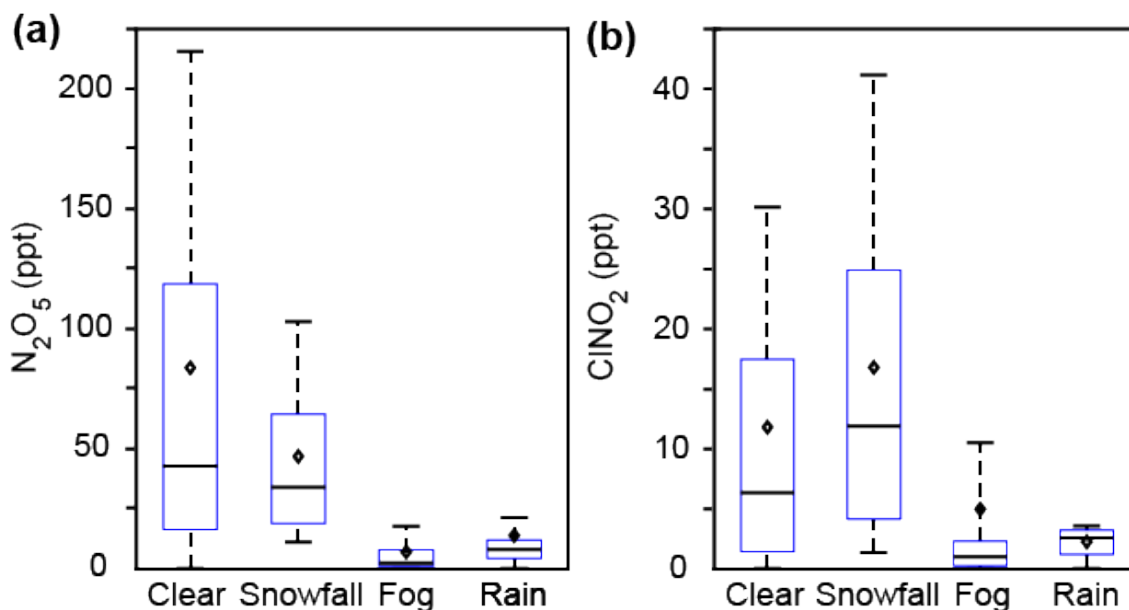
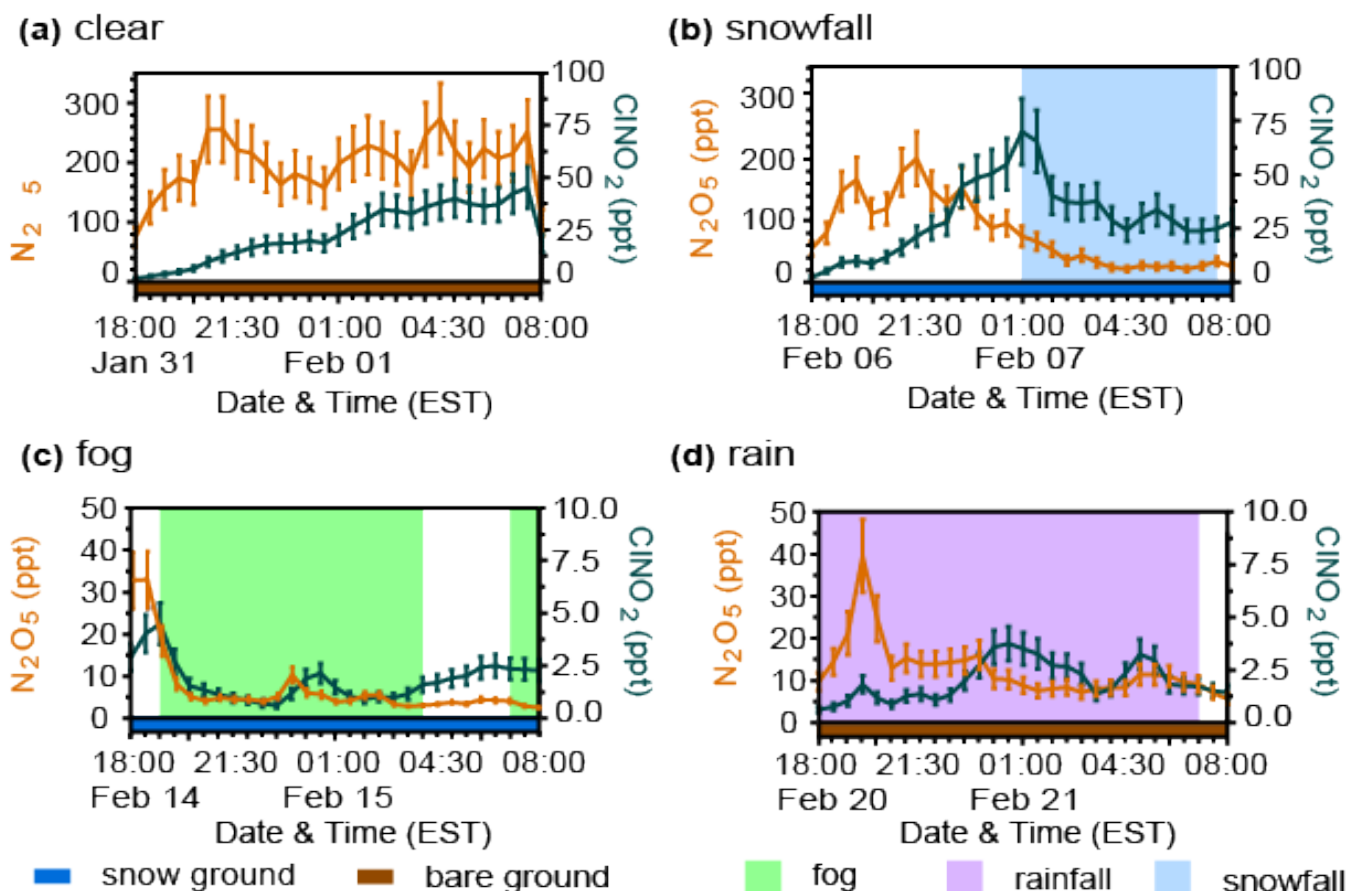


**Figure 2:** Box plots showing 30 min averaged mole ratios of (a)  $\text{N}_2\text{O}_5$  and (b)  $\text{ClNO}_2$  during clear conditions and weather events (snowfall, fog, and rain) from January 20 - February 24. Bars represent the 10<sup>th</sup>, 50<sup>th</sup>, and 90<sup>th</sup> percentiles, boxes represent the 25<sup>th</sup> and 75<sup>th</sup> percentiles, and diamonds represent the means. Only nighttime data between 18:00 and 08:00 EST are included. Data during all weather events (snowfall, fog, rain) are significantly different ( $p < 0.05$ , t-test) from clear conditions.

The average  $\text{ClNO}_2$  mole ratios were  $16.8 \pm 0.7$  ppt during snowfall,  $11.8 \pm 0.7$  ppt in clear conditions,  $5.0 \pm 0.6$  ppt during fog, and  $2.27 \pm 0.06$  ppt when raining (Fig. 2). In comparison to clear conditions, average  $\text{ClNO}_2$  mole ratios were  $6.8 \pm 0.9$  ppt (2.4 times) and  $9.5 \pm 0.7$  ppt (5.2 times) lower during fog and rain, respectively. Lower average abundances of  $\text{ClNO}_2$  during fog and rainfall, compared to clear conditions, are consistent with previous observations (Osthoff et al., 2018) and were likely due to scavenging either of  $\text{ClNO}_2$  directly or its precursors ( $\text{R}_2$ ). In contrast, average  $\text{ClNO}_2$  mole ratios were  $5 \pm 1$  ppt (1.4 times) higher during snowfall than clear conditions. This result is surprising, considering that its precursor,  $\text{N}_2\text{O}_5$ , showed lower mole ratios, on average, during snowfall in comparison to clear conditions. Particle-phase chloride and nitrate concentrations were not statistically significantly different between clear and snowfall conditions ( $p = 0.96$  and  $0.08$ , respectively), nor were aerosol number or surface area concentrations ( $p = 0.06$  and  $0.31$ , respectively), as discussed in Sect. 3.4.



245 To further examine the behavior of  $\text{N}_2\text{O}_5$  and  $\text{ClNO}_2$  in response to snowfall, rain, and fog, we  
 present four nocturnal case study periods that were representative of the four different weather conditions  
 (clear, snowfall, fog, and rain) observed during the campaign (**Fig. 3**). Additional data specific to the case  
 studies is provided in the supplemental material (**Table S2, Fig. S4-S6**). The clear case night of Jan 31-  
 Feb 01 had no precipitation or fog, an average  $u^*$  of  $0.16 \pm 0.01 \text{ m s}^{-1}$  (campaign average  $u^*$  was  
 250  $0.150 \pm 0.004 \text{ m s}^{-1}$  during nighttime clear conditions), and bare ground.  $\text{N}_2\text{O}_5$  was fairly stable around 200  
 ppt (average  $200 \pm 16$  ppt, range 75-274 ppt) throughout the night, with  $\text{ClNO}_2$  increasing steadily between  
 18:00-07:30 from 1.5 ppt to 45 ppt (average  $23 \pm 5$  ppt, range 0.6-4.5 ppt) (**Fig. 3a**).



255 **Figure 3:** Four example case study periods are shown, corresponding to (a) clear conditions, (b) snowfall,  
 (c) fog, and (d) rainfall. The 30-min averaged abundances of  $\text{N}_2\text{O}_5$  (orange) and  $\text{ClNO}_2$  (dark blue) are  
 displayed for each case. Error bars represent propagated uncertainties. The shading below the x-axis  
 represents ground cover – snow (blue) or bare ground (brown).



To discuss changes in gas-phase concentrations during precipitation and fog, we apply the concept of solution equilibrium to the surface layer of a drop (i.e. a rain or fog droplet) in terms of a local equilibrium between the analyte in the gas-phase and the analyte dissolved in the surface layer (Pruppacher and Klett, 1997). This equilibrium can then be described using Henry's law and Henry's law constants ( $K_H$ ). For  $N_2O_5$ , fast, irreversible hydrolysis is assumed, equivalent to an infinite effective  $K_H$  (Jacob, 1986; Sander, 2015). For  $ClNO_2$ , the  $K_H=4.5\times 10^{-4} \text{ mol m}^{-3} \text{ Pa}^{-1}$  at standard temperature (Frenzel et al., 1998; Sander, 2015), showing little variation between  $\sim 278$  and  $294$  K. Converting the  $K_H$  for  $ClNO_2$  to its dimensionless Henry solubility, as in Sander et al. (2015), gives a unitless ratio between the aqueous and gas phases of  $>1$  at temperatures above freezing. This means, at equilibrium,  $ClNO_2$  is expected to be more abundant in the aqueous-phase than in the gas-phase. The fast irreversible hydrolysis assumed for  $N_2O_5$  makes it more water soluble than  $ClNO_2$ ; therefore, scavenging by liquid droplets is expected for both gas-phase  $N_2O_5$  and  $ClNO_2$ , but to a greater extent for  $N_2O_5$ . Here, we examine the fog and rainfall case studies to characterize the effects of scavenging by liquid droplets on  $N_2O_5$  and  $ClNO_2$  abundance.

For the fog case night of Feb 14-15, fog was present from 19:00-04:00 and 07:00-08:00 (**Fig. 3c**). This case had an average  $u^*$  of  $0.18\pm 0.02 \text{ m s}^{-1}$  (campaign average  $u^*$  was  $0.162\pm 0.007 \text{ m s}^{-1}$  during nighttime fog) and snow-covered ground.  $N_2O_5$  decreased rapidly from its maximum of 32 ppt at 18:00 and fell to a local minimum of 2.3 ppt at 22:30; it then remained low in abundance ( $<10$  ppt) for the rest of the night, reaching its true minimum of 1.1 ppt at 03:30.  $ClNO_2$  reached its maximum of 4.5 ppt at 19:00 and then decreased coincident with the appearance of fog and remained low in abundance ( $<3$  ppt) for the rest of the night, reaching its minimum of 0.6 ppt at 23:00. Considering the first hour after the fog onset (19:00-20:00),  $N_2O_5$  mole ratios decreased from 16.6 ppt to 3.4 ppt (decrease of 13.2 ppt or 80%) and  $ClNO_2$  mole ratios decreased from 4.5 ppt to 1.6 ppt (decrease of 2.9 ppt or 64%). During this one hour fog period, the calculated scavenging coefficients ( $E_2$ ) for  $N_2O_5$  and  $ClNO_2$  were  $2.2\times 10^{-4} \text{ s}^{-1}$  and  $1.8\times 10^{-4} \text{ s}^{-1}$ , respectively (**Table 2**). For context, sparingly soluble gases, such as  $SO_2$ , have scavenging coefficients of  $5\times 10^{-6}$ - $6\times 10^{-5} \text{ s}^{-1}$ , and more soluble gases, like  $NH_3$  and  $HNO_3$ , have scavenging coefficients of  $1\times 10^{-4}$ - $3\times 10^{-4} \text{ s}^{-1}$  (Pruppacher and Klett, 1997). The calculated  $N_2O_5$  scavenging coefficient is consistent with the expectation based on solubility, but the calculated  $ClNO_2$  scavenging



coefficient is higher than expected, suggesting that another process may have contributed to its rapid decrease.

**Table 2.** Gas-phase scavenging coefficients calculated using E2 for  $\text{N}_2\text{O}_5$  and  $\text{ClNO}_2$  during case studies (snowfall, fog, and rain).

Case Period	$\text{N}_2\text{O}_5$ ( $\text{s}^{-1}$ )	$\text{ClNO}_2$ ( $\text{s}^{-1}$ )
Snowfall (Feb 07, 01:00-02:00)	$7.9 \times 10^{-5}$	$1.2 \times 10^{-4}$
Fog (Feb 14, 19:00- 20:00)	$2.2 \times 10^{-4}$	$1.8 \times 10^{-4}$
Rainfall (Feb 20, 18:00-19:00)	$1.9 \times 10^{-4}$	$1.5 \times 10^{-4}$

290 Similarly, the rainfall case night of Feb 20-21 was characterized by rainfall from 18:00-07:00 and bare ground (**Fig. 3d**). While sonic anemometer data were unavailable on this night, elevated wind speeds of 2.2-8.9  $\text{m s}^{-1}$  (average= $5.0 \pm 0.5 \text{ m s}^{-1}$ ) (**Fig. S4** and **Table S2**) are consistent with increased turbulence, with  $u^*$  likely greater than 0.25  $\text{m s}^{-1}$  for the duration of the night (**Fig. S5**).  $\text{N}_2\text{O}_5$  decreased rapidly from its maximum of 40 ppt at 19:30, stabilized at  $\sim 15$  ppt from 20:30-00:00, and then decreased again to  $\sim 10$   
295 ppt until 08:00.  $\text{ClNO}_2$  reached its maximum of 3.7 ppt at 00:30, with a second local maximum of 3.0 ppt at 05:30;  $\text{ClNO}_2$  was  $< 2$  ppt before 23:30 and after 06:00. The period of 19:30-20:30 was chosen for further analysis to capture a period of more intense rainfall; during this period, rain fell at approximately 0.1  $\text{in hr}^{-1}$ . For time periods before and after this window (e.g. 18:00-19:00 and 21:15-21:45), Weather Underground reported the weather condition as “light rain,” defined as  $< 2.5 \text{ mm (0.098 in) hr}^{-1}$ . Although  
300 precipitation rates were used to inform time periods used for calculations during the rainfall case, a more thorough characterization of scavenging with respect to precipitation rate and intensity is beyond the scope of this discussion. During this 19:30-20:30 rainfall period, the calculated scavenging coefficients for  $\text{N}_2\text{O}_5$  and  $\text{ClNO}_2$  were  $1.9 \times 10^{-4} \text{ s}^{-1}$  and  $1.5 \times 10^{-4} \text{ s}^{-1}$ , respectively, similar to the fog case (**Table 2**).



The observations during the fog and rainfall case studies reinforce the trends observed for the campaign  
305 averages (**Fig. 2-3**) and illustrate the importance of scavenging by liquid droplets.

The snowfall case night of Feb 06-07 was characterized by snowfall from 01:00-07:30 (**Fig. 3b**),  
an average  $u^*$  of  $0.06 \pm 0.01 \text{ m s}^{-1}$  (campaign average  $u^*$  was  $0.129 \pm 0.004 \text{ m s}^{-1}$  during nighttime snowfall),  
and snow-covered ground.  $\text{N}_2\text{O}_5$  reached its maximum of 201 ppt at 21:30 and then gradually decreased  
throughout the rest of the night; it reached its minimum of 22 ppt at 04:00 and then remained low in  
310 abundance (22-34 ppt).  $\text{ClNO}_2$  reached its maximum of 70 ppt at 01:00, the same time that snowfall  
began, and then decreased steadily to its minimum of 24 ppt at 04:30, after which it also remained low in  
abundance (24-34 ppt). Considering the first hour after snowfall onset (01:00-02:00),  $\text{N}_2\text{O}_5$  mole ratios  
decreased from 74.8 ppt to 53.6 ppt (decrease of 21.2 ppt or 28%) and  $\text{ClNO}_2$  mole ratios decreased from  
69.8 ppt to 40.3 ppt (decrease of 29.5 ppt or 42%). During this one hour period, the calculated scavenging  
315 coefficients for  $\text{N}_2\text{O}_5$  and  $\text{ClNO}_2$  were  $7.9 \times 10^{-5} \text{ s}^{-1}$  and  $1.2 \times 10^{-4} \text{ s}^{-1}$ , respectively (**Table 2**). Reduced  
uptake of  $\text{N}_2\text{O}_5$  onto ice, compared to liquid water, is expected (Gržinić et al., 2017; Lopez-Hilfiker et al.,  
2012) and likely explains the lower scavenging coefficient for snowfall compared to rainfall and fog. The  
higher  $\text{ClNO}_2$  scavenging coefficient for snowfall suggests contribution from another process, leading to  
a faster than expected loss of  $\text{ClNO}_2$ .

320 The observations during the snowfall case are also consistent with campaign-wide observations  
(**Fig. 2-3**). In comparison to the clear case, the snowfall case night shows that  $\text{N}_2\text{O}_5$  mole ratios were  
generally lower during snowfall (by 2.1 times, on average), whereas  $\text{ClNO}_2$  mole ratios were typically  
higher during snowfall (by 1.4 times, on average). Even though the clear case study had the highest mole  
ratios of  $\text{N}_2\text{O}_5$ , the snowfall case study had the highest mole ratios of  $\text{ClNO}_2$  (**Fig. 3** and **Table S2**). The  
325 clear and snowfall case studies differed in both ground cover and air turbulence, with lower turbulence  
intensity (average= $0.06 \pm 0.01 \text{ m s}^{-1}$ ) and snow-covered ground observed during the snowfall case and  
intermediate turbulence intensity (average= $0.16 \pm 0.01 \text{ m s}^{-1}$ ) and bare ground observed during the clear  
case study.

For scavenging by ice and snow, gases can adsorb onto the surface and dissolve in the quasi-liquid  
330 layer, which is thicker at temperatures near freezing (Pruppacher and Klett, 1997). After uptake onto the  
surface, no theoretical framework, to our knowledge, is available to describe the diffusional uptake of

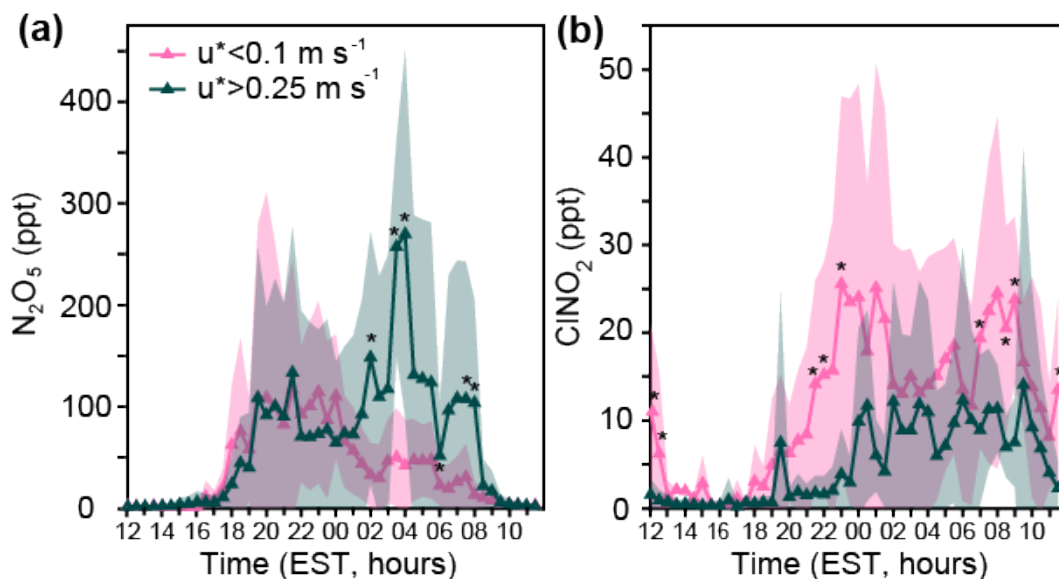




gases by frozen precipitation; however, it is thought to be less efficient in comparison to the liquid phase (Conklin and Bales, 1993). This is supported by our calculations of decreased scavenging efficiencies (**Table 2**) during snowfall, in comparison to rainfall and fog. Interestingly, ClNO<sub>2</sub> appears to have been  
335 scavenged more efficiently by snowfall than N<sub>2</sub>O<sub>5</sub>. Although more efficient scavenging by snowfall, in comparison to rainfall, has been reported previously for gas-phase HNO<sub>3</sub> (Chang, 1984), limited knowledge exists about gas-phase scavenging of N<sub>2</sub>O<sub>5</sub> and ClNO<sub>2</sub>, suggesting the need to study this further. Additional effects on the abundances of N<sub>2</sub>O<sub>5</sub> and ClNO<sub>2</sub> are further investigated in the following sections.

### 340 **3.2 Effects of turbulence**

Turbulent mixing (quantified here using friction velocity,  $u^*$ , **E1**) affects abundances of surface-level trace gases (Stull, 1988). Stronger turbulent mixing promotes vertical transport, and weaker turbulent mixing keeps trace gases near the ground (Stull, 1988). Turbulence regimes were divided within the context of our study to allow subsequent analysis by binning with sufficient data in each bin. Here,  
345 lower turbulence refers to  $u^* < 0.1 \text{ m s}^{-1}$ , higher turbulence is  $u^* > 0.25 \text{ m s}^{-1}$ , and mid-turbulence refers to  $0.1 < u^* < 0.25 \text{ m s}^{-1}$ . Lower turbulence occurred 39% of the time, mid-turbulence occurred 42% of the time, and higher turbulence occurred 14% of the time (**Fig. S3**). For context, typical  $u^*$  values range from near  $0 \text{ m s}^{-1}$  during calm conditions to  $1 \text{ m s}^{-1}$  during strong winds; moderate wind values often have  $u^*$  values near  $0.5 \text{ m s}^{-1}$  (Stull, 2017). Lower turbulence intensity, in general, was observed during our  
350 study, which focuses on nighttime measurements during winter. We investigate the effects of atmospheric turbulence on the abundances of ClNO<sub>2</sub> and N<sub>2</sub>O<sub>5</sub> by comparing lower ( $u^* < 0.1 \text{ m s}^{-1}$ ) and higher turbulence ( $u^* > 0.25 \text{ m s}^{-1}$ ) periods across 30 min averaged periods for a full diel cycle during the entire campaign (**Fig. 4**).



355 **Figure 4.** Diel patterns of 30 min averaged (a)  $\text{N}_2\text{O}_5$  and (b)  $\text{ClNO}_2$ , binned by lower ( $u^* < 0.1 \text{ m s}^{-1}$ ) and higher ( $u^* > 0.25 \text{ m s}^{-1}$ ) friction velocities. Shading represents one standard deviation. Asterisks represent statistically significant (t-test) differences at the  $p < 0.05$  level between the lower and higher friction velocity bins for each 30 min period from January 20-February 24 (excluding February 20-21 when the sonic anemometer was not operational).

360 Significantly higher ( $p < 0.05$ , t-test)  $\text{N}_2\text{O}_5$  mole ratios were observed under higher turbulence conditions at 02:00, 03:30, 04:00, 06:00, and 07:30, and 08:00 (**Fig. 4a**). These statistically significant time points correspond to, on average, 5.9 times higher  $\text{N}_2\text{O}_5$  mole ratios during higher turbulence conditions, in comparison to lower turbulence conditions. Considering the entire period of 02:00-08:00,  $\text{N}_2\text{O}_5$  mole ratios were 4.0 times higher, on average, during higher turbulence conditions in comparison  
365 to lower turbulence conditions. Before 02:00,  $\text{N}_2\text{O}_5$  mole ratios were not statistically significantly different between lower and higher turbulence conditions, but were 1.2 times higher during higher turbulence conditions, on average. Considering the nighttime period as a whole (18:00-08:00),  $\text{N}_2\text{O}_5$  mole ratios were higher by  $24 \pm 4 \text{ ppt}$  (1.6-fold) during higher turbulence, in comparison to lower turbulence conditions.

370  $\text{NO}_3$ , a reactant necessary to produce  $\text{N}_2\text{O}_5$  (**R3**), is sensitive to changes in  $\text{NO}$  and  $\text{O}_3$  levels; in particular, reaction of  $\text{NO}_3$  by  $\text{NO}$  (**R7**) is an important loss process at night and results in lower  $\text{N}_2\text{O}_5$  production (Asaf et al., 2010). Therefore, when  $\text{NO}$  is emitted and confined near the ground in the stable



nocturnal boundary layer,  $\text{NO}_3$  has a short near-surface lifetime, thereby limiting  $\text{N}_2\text{O}_5$  levels (Wang et al., 2006). Such stable conditions can be the result of nocturnal temperature inversions, which are often  
375 observed in mountain-valley wind systems (Hahn, 1981) and during wintertime in the mid-latitudes (Leblanc and Hauchecorne, 1997). As expressed by kinematic heat flux less than  $0 \text{ K m s}^{-1}$ , a nocturnal temperature inversion was observed every night of the study (**Fig. S7**). Reduced  $\text{N}_2\text{O}_5$  mole ratios were observed during nighttime lower turbulence ( $u^* < 0.1 \text{ m s}^{-1}$ ) compared to higher turbulence ( $u^* > 0.25 \text{ m s}^{-1}$ ) periods (averages of  $40 \pm 2 \text{ ppt}$  and  $64 \pm 3 \text{ ppt}$ , respectively). It is important to note that we do not expect  
380 the soil to be a significant  $\text{NO}_x$  source; a wintertime study by Seok et al. (2015) in northern Michigan showed no measurable soil  $\text{NO}$  flux, with  $\text{NO}_2$  only released from the snow during daytime from nitrate photolysis. Vehicle  $\text{NO}_x$  emissions from the nearby roadway location  $\sim 80 \text{ m}$  away (McNamara et al., 2021) are suggested to control the magnitude of the nighttime titration effect at the field site, as few time periods overnight were statistically different in  $\text{O}_3$  mole ratios between the lower and higher turbulence  
385 conditions, on average (**Fig. S8**). However, despite 39% of the nighttime periods being characterized by lower turbulence ( $u^* < 0.1 \text{ m s}^{-1}$ ) (**Fig. S3**),  $\text{N}_2\text{O}_5$  mole ratios during the full campaign ranged from 0.15–702 ppt (mean  $44 \pm 4 \text{ ppt}$ ) during nighttime, resulting in the observed  $\text{ClNO}_2$  production even under lower turbulence conditions.

In contrast to its precursor  $\text{N}_2\text{O}_5$ ,  $\text{ClNO}_2$  shows significantly higher ( $p < 0.05$ , t-test) average mole  
390 ratios under lower turbulence ( $u^* < 0.1 \text{ m s}^{-1}$ ) conditions at 21:30, 22:00, 23:00, and 07:00 (**Fig. 4b**). These statistically significant time periods correspond to an average 6.3 times higher  $\text{ClNO}_2$  mole ratio during lower turbulence conditions, in comparison to higher turbulence conditions. Considering the entire period of 21:30–07:30,  $\text{ClNO}_2$  mole ratios were 3.6 times higher, on average, during lower turbulence conditions in comparison to higher turbulence conditions. Considering the nighttime period as a whole (18:00–  
395 08:00),  $\text{ClNO}_2$  mole ratios were higher by  $7 \pm 1 \text{ ppt}$  (2.6-fold) during lower turbulence, in comparison to higher turbulence conditions. To examine the differing trends in  $\text{N}_2\text{O}_5$  and  $\text{ClNO}_2$  at lower turbulence ( $u^* < 0.1 \text{ m s}^{-1}$ ), we investigated the influence of ground cover.



### 3.3 Effects of ground cover

There were no statistically significant ( $p < 0.05$ , t-test) differences in the average abundances of  $\text{N}_2\text{O}_5$  over the diel period for snow-covered vs bare ground (**Fig. 5a**). This is consistent with measurements of similar net negative (deposition) fluxes of  $\text{N}_2\text{O}_5$  over both snow-covered and bare ground (McNamara et al., 2021). In contrast, **Figure 5b** shows significantly higher ( $p < 0.05$ , t-test) average  $\text{ClNO}_2$  mole ratios observed over snow-covered ground at 19:30-22:00, 23:00-00:00, 01:00-01:30, 03:00, and 07:30. These statistically significant time points correspond to, on average, 3.5 times higher  $\text{ClNO}_2$  mole ratios over snow-covered ground, in comparison to bare ground. Considering the entire period of 19:30-07:30,  $\text{ClNO}_2$  mole ratios were 2.8 times higher, on average, over snow covered ground in comparison to bare ground. This is consistent with measurements of typical net positive (production) fluxes of  $\text{ClNO}_2$  over snow-covered ground, and with field-based chamber experiments showing that  $\text{ClNO}_2$  can be produced from the reaction of  $\text{N}_2\text{O}_5$  on the saline snowpack (McNamara et al., 2021).

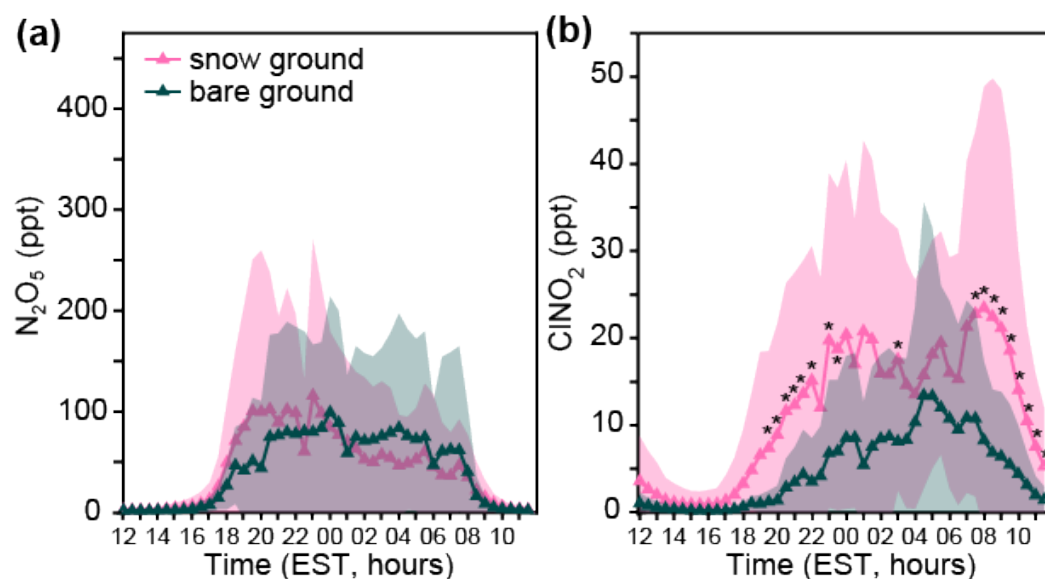


**Figure 5.** Diel patterns of 30 min averaged mole ratios of (a)  $\text{N}_2\text{O}_5$  and (b)  $\text{ClNO}_2$  binned by snow-covered and bare ground conditions from January 20 to February 24. Shading represents one standard deviation. Asterisks represent statistically significant (t-test) differences at the  $p < 0.05$  level between snow-covered and bare ground for each 30 min time period.



### 3.4 Competing effects of environmental conditions

Many of the environmental conditions discussed (precipitation/fog, turbulence regimes, and snow-covered/bare ground) occur simultaneously, and as a result, are difficult to discuss in isolation. As shown in the snow case study (**Fig. 3b**), ClNO<sub>2</sub> was highest when both snow-covered ground and lower  
420 turbulence ( $u^* < 0.1 \text{ m s}^{-1}$ ) conditions were present simultaneously. Overall, 73% of nighttime lower turbulence ( $u^* < 0.1 \text{ m s}^{-1}$ ) occurred over snow-covered ground; in comparison, 67% of nighttime higher turbulence ( $u^* > 0.25 \text{ m s}^{-1}$ ) occurred over bare ground (**Fig. S3**). Given that statistically higher mole ratios of ClNO<sub>2</sub> were observed under lower turbulence conditions and over snow-covered ground, as shown by campaign averages (**Fig. 2**) and the snowfall case study (**Fig. 3b**), it is also useful to consider how often  
425 these conditions coincide during different types of weather events. Lower turbulence ( $u^* < 0.1 \text{ m s}^{-1}$ ) and snow-covered ground were observed simultaneously for 24%, 48%, 26%, and 2% of the time during clear, snowfall, fog, and rainfall conditions, respectively (**Fig. S3**). The prevalence of lower turbulence and snow-covered ground during snowfall likely also contributes to the result that mole ratios of ClNO<sub>2</sub> were highest on average during snowfall (**Fig. 2**), in addition to snow-phase ClNO<sub>2</sub> production.

430 We also discuss N<sub>2</sub>O<sub>5</sub> and ClNO<sub>2</sub> levels in the context of observed PM<sub>2.5</sub> Cl<sup>-</sup> and NO<sub>3</sub><sup>-</sup> concentrations, as well as air temperatures and relative humidity, for which the averages are given during clear conditions and each type of weather event in **Table 3**, with additional data provided in **Table S2**. As shown by Bertram and Thornton (2009), both N<sub>2</sub>O<sub>5</sub> uptake and the product yield of ClNO<sub>2</sub> are expected to increase with increasing particulate chloride concentrations. The effects of increased  
435 particulate chloride are two-fold, with less N<sub>2</sub>O<sub>5</sub> expected to remain in the gas-phase due to the increased uptake, and a higher ClNO<sub>2</sub> abundance expected because of the higher product yield. PM<sub>2.5</sub> Cl<sup>-</sup> concentrations were not statistically significantly different between snowfall and clear conditions ( $p=0.96$ , t-test), between snowfall and rainfall ( $p=0.11$ ), or between clear and rainfall conditions ( $p=0.10$ ) (**Fig. 6a**).

440 PM<sub>2.5</sub> Cl<sup>-</sup> concentrations were statistically significantly higher during fog, in comparison to clear conditions ( $p < 0.05$ ), with the average concentration during fog higher by  $0.20 \pm 0.01 \mu\text{g m}^{-3}$  (1.8 times) on average. Although total submicron aerosol number concentrations were not statistically significantly different between clear and fog conditions ( $p=0.88$ ), they were significantly higher ( $p < 0.05$ ) during fog



445 compared to clear conditions, by  $52 \pm 7 \mu\text{m}^2 \text{cm}^{-3}$  (1.3 times) with respect to campaign averages (**Fig. S11-**  
**S12**).  $\text{N}_2\text{O}_5$  uptake is expected to increase with increasing aerosol surface area concentration (Bertram  
and Thornton, 2009), but despite elevated  $\text{PM}_{2.5} \text{Cl}^-$  and aerosol surface area concentrations during fog,  
average  $\text{ClNO}_2$  abundance was lower during fog in comparison to clear conditions (**Fig. 2**). We expect  
that, during fog, elevated RH (**Fig. 6d**) and the higher gas-phase scavenging coefficient (**Table 2**) have a  
greater impact on  $\text{ClNO}_2$  abundance than  $\text{PM}_{2.5} \text{Cl}^-$  concentration or aerosol surface area concentration.  
450 Production of particle-phase chloride, presumed to be from uptake of gas-phase  $\text{HCl}$ , has been observed  
previously during fog/haze events in highly polluted urban India (Gunthe et al., 2021) and near an  
incinerator (Johnson et al., 1987). However, for this study in Kalamazoo, MI, road salting seems more  
plausible as the dominant source of increased  $\text{PM}_{2.5} \text{Cl}^-$  during wintertime fog.

455

**Table 3.** Mean ( $\pm 95\%$  confidence interval)  $\text{PM}_{2.5} \text{Cl}^-$  and  $\text{NO}_3^-$  concentrations, temperatures, and relative humidities during each type of weather event (clear, snowfall, fog, and rain).

Condition	$[\text{Cl}^-]$ ( $\mu\text{g m}^{-3}$ )	$[\text{NO}_3^-]$ ( $\mu\text{g m}^{-3}$ )	Temperature (K)	Relative Humidity (%)
Clear	$0.257 \pm 0.007$	$0.95 \pm 0.04$	$270.8 \pm 0.3$	$75.0 \pm 0.5$
Snowfall	$0.258 \pm 0.006$	$0.81 \pm 0.03$	$265.8 \pm 0.2$	$83.0 \pm 0.3$
Fog	$0.456 \pm 0.008$	$1.38 \pm 0.04$	$276.7 \pm 0.2$	$93.7 \pm 0.3$
Rain	$0.22 \pm 0.01$	$0.126 \pm 0.007$	$282.1 \pm 0.2$	$90.2 \pm 0.4$

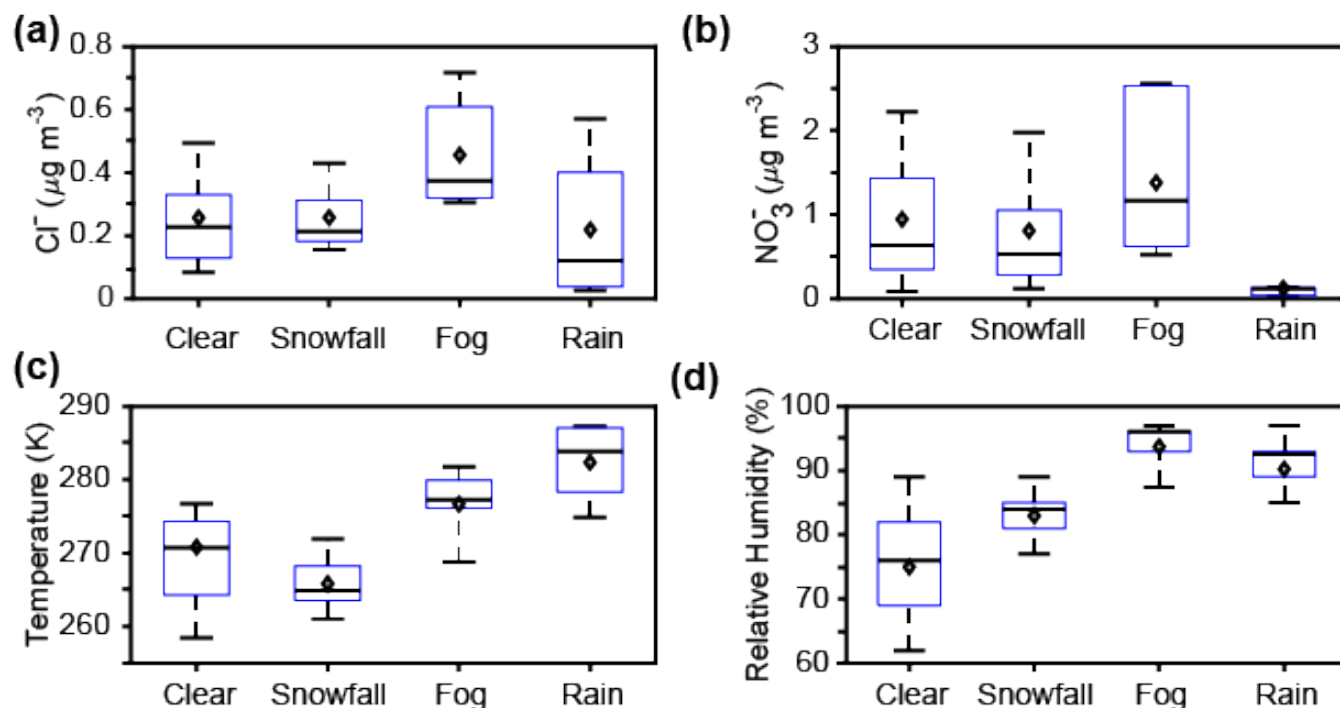


**Figure 6.** Box plots showing 30 min averaged  $\text{PM}_{2.5}$  (a) chloride and (b) nitrate concentrations, (c) air temperatures and (d) relative humidity values during clear conditions and weather events (snowfall, fog, and rain). Bars represent the 10<sup>th</sup>, 50<sup>th</sup>, and 90<sup>th</sup> percentiles, boxes represent the 25<sup>th</sup> and 75<sup>th</sup> percentiles, and diamonds represent the means. Only nighttime data, between 18:00 and 08:00 EST, are included.

$\text{N}_2\text{O}_5$  uptake results in particulate nitrate production; however, the efficiency of  $\text{N}_2\text{O}_5$  uptake to particles decreases with increasing particulate nitrate concentrations (Bertram and Thornton, 2009).  $\text{PM}_{2.5}$   $\text{NO}_3^-$  concentrations were not statistically significantly different between snowfall and clear conditions ( $p=0.08$ ).  $\text{PM}_{2.5}$   $\text{NO}_3^-$  concentrations during rain were statistically significantly lower, in comparison to clear conditions ( $p<0.05$ ), with average concentrations lower by  $0.82\pm 0.04 \mu\text{g m}^{-3}$  (7.5 times) (Fig 6b). This is attributed to increased scavenging and wet deposition during rainfall, compared to snowfall, which is consistent with previous observations and calculations of scavenging coefficients for nitrate during rainfall and snowfall in winter in New York (Sperber and Hameed, 1986).

Particles rich in nitrate have been observed previously in the droplet mode (0.8–0.9  $\mu\text{m}$ ) during fog events; these particles form following fog droplet evaporation after nitrate production from  $\text{HNO}_3$  and  $\text{N}_2\text{O}_5$  uptake (Dall'Osto et al., 2009; Ge et al., 2012). In contrast to rain and snowfall,  $\text{PM}_{2.5}$   $\text{NO}_3^-$



concentrations were statistically significantly higher during fog, in comparison to clear conditions ( $p < 0.05$ ), by  $0.43 \pm 0.06 \mu\text{g m}^{-3}$  ( $160 \pm 20$  ppt; 1.5 times) (**Figs. 6b** and **S10**). The increase in  $\text{PM}_{2.5} \text{NO}_3^-$  is likely, in part, the result of heterogeneous uptake and hydrolysis of  $\text{N}_2\text{O}_5$  (Brown et al., 2004; Osthoff et al., 2006), consistent with our observation of the lower average  $\text{N}_2\text{O}_5$  mole ratios during fog (**Fig. 2**). On average,  $\text{N}_2\text{O}_5$  was  $76 \pm 5$  ppt lower during fog compared to clear conditions (**Figs. 2** and **S10**). In addition to  $\text{N}_2\text{O}_5$ , gas-phase  $\text{HNO}_3$  uptake likely also contributed to the increased  $\text{PM}_{2.5} \text{NO}_3^-$  observed during fog. Due to its high solubility,  $\text{HNO}_3$  is predicted to be efficiently scavenged by fog droplets ( $>90$ -100% removal) (Ervens, 2015). However, due poor background characterization and low signals (**Fig. S9**), a quantitative evaluation of  $\text{HNO}_3$  contribution to nitrate production was not possible. It is likely that both  $\text{N}_2\text{O}_5$  and  $\text{HNO}_3$  uptake, followed by aqueous-phase nitrate formation, led to the increased  $\text{PM}_{2.5} \text{NO}_3^-$  observed during fog. To conclude our examination of  $\text{N}_2\text{O}_5$  and  $\text{ClNO}_2$  abundances during different weather conditions, we examine trends in temperature and RH during clear conditions, snowfall, rainfall, and fog. Temperature was statistically significantly different between clear conditions and snowfall, fog, and rainfall, respectively ( $p < 0.05$ , t-test) (**Fig. 6c**). The average nighttime temperature was  $265.8 \pm 0.2$  K,  $270.8 \pm 0.3$  K,  $276.7 \pm 0.2$  K, and  $282.1 \pm 0.2$  K during snowfall, clear conditions, fog, and rainfall, respectively. Since lower temperatures favor  $\text{N}_2\text{O}_5$  production in its thermal equilibrium (**R3**) (Asaf et al., 2010; Wagner et al., 2013), and because snowfall conditions had the lowest average temperature (**Fig. 6c**), we would expect  $\text{N}_2\text{O}_5$  to be highest in abundance during snowfall if other processes did not dominate. The average  $\text{N}_2\text{O}_5$  mole ratios were highest during clear conditions (**Fig. 2**), highlighting the importance of other effects, including wet scavenging.

Relative humidity was statistically significantly different between clear conditions and snowfall, fog, and rainfall, respectively ( $p < 0.05$ ) (**Fig. 6d**). The average nighttime RH was  $75.0 \pm 0.5\%$ ,  $83.0 \pm 0.3\%$ ,  $90.2 \pm 0.4\%$ , and  $93.7 \pm 0.3\%$ , during clear conditions, snowfall, rainfall, and fog, respectively. Higher RH values typically allow less  $\text{N}_2\text{O}_5$  to remain in the gas phase (e.g. Osthoff et al., 2006; Sommariva et al., 2009; Wood et al., 2005). The pattern of  $\text{N}_2\text{O}_5$  abundance was anticorrelated with RH (**Fig. 2** and **Fig. 6d**). This reinforces that  $\text{N}_2\text{O}_5$  heterogeneous uptake is strongly RH dependent (Bertram et al., 2009; Davis et al., 2008; Evans and Jacob, 2005; Griffiths and Cox, 2009; Hallquist et al., 2003), with enhanced uptake and removal occurring when RH and aerosol liquid water content are high.





## 4 Conclusions

We examined the impacts of precipitation (rain, snowfall) and fog, atmospheric turbulence, and ground cover (snow-covered vs bare) on near-surface ( $\sim 1.5$  m above ground)  $\text{N}_2\text{O}_5$  and  $\text{ClNO}_2$  observed during January to February 2018 in Kalamazoo, Michigan. While  $\text{N}_2\text{O}_5$  was observed during all nights of the campaign,  $\text{N}_2\text{O}_5$  mole ratios were lowest during periods of lower turbulence ( $u^* < 0.1 \text{ m s}^{-1}$ ) due to titration of  $\text{NO}_3$  and  $\text{O}_3$  by  $\text{NO}$  in the stable nocturnal boundary layer.  $\text{N}_2\text{O}_5$  mole ratios were not statistically significantly different over bare versus snow-covered ground.  $\text{ClNO}_2$  mole ratios were highest during periods of lower turbulence and snow-covered ground. This is consistent with  $\text{N}_2\text{O}_5$  depositing and reacting with the chloride-containing snowpack to produce  $\text{ClNO}_2$ . Indeed, vertical gradient measurements during the same study showed  $\text{N}_2\text{O}_5$  deposition and an average positive (production)  $\text{ClNO}_2$  flux over snow-covered ground, and snow chamber experiments showed that synthesized  $\text{N}_2\text{O}_5$  reacted with the local saline snow to produce  $\text{ClNO}_2$  (McNamara et al., 2021). This finding is also consistent with the laboratory study by Lopez-Hilfiker et al. (2012), which showed that  $\text{N}_2\text{O}_5$  can react on halide-doped ice surfaces to produce  $\text{ClNO}_2$ . The contribution of the snowpack as a common  $\text{ClNO}_2$  source across the field campaign has important implications for the vertical distribution of atmospheric chlorine chemistry, which will be examined through one-dimensional modeling for comparison with chloride-containing aerosol particles that serve as a major  $\text{ClNO}_2$  source.

On average, both  $\text{N}_2\text{O}_5$  and  $\text{ClNO}_2$  abundances were lowest during rainfall and fog due to scavenging. While both species are water soluble,  $\text{N}_2\text{O}_5$  undergoes more efficient scavenging by liquid droplets, particularly fog, as expected based on its higher Henry's Law constant and uptake coefficient (Fickert et al., 1998; Gržinić et al., 2017).  $\text{N}_2\text{O}_5$  uptake by fog droplets likely contributed to observed elevated  $\text{PM}_{2.5} \text{NO}_3^-$  during fog events. In comparison to rain and fog, the gas-phase scavenging coefficients calculated for the snowfall case study were less efficient. Little is known about  $\text{N}_2\text{O}_5$  and  $\text{ClNO}_2$  scavenging by precipitation, supporting the need for further investigation of this process. Overall, our results show that observational and modelling studies of only clear conditions miss important processes including scavenging, fog nitrate production, and the snowpack as a  $\text{ClNO}_2$  source. This is important as rainfall, fog, and snowfall occurred during 28% of the nighttime periods, representing a significant portion that contributes significantly to the variability observed during this winter study.



## Acknowledgements

530 This study was supported by the US National Science Foundation Atmospheric Chemistry  
program (AGS-1738588 and PLR-1417914), an Alfred P. Sloan Foundation Research Fellowship in  
Chemistry, and the University of Michigan. J.E. acknowledges funding from the Swiss National Science  
Foundation (155999). We thank Andrew Ault, Nicholas Ellsworth, and Matthew McNamara for  
assistance in preparing the mobile laboratory, Angela Raso, Peter Peterson, Guy Burke, and Alexa Watson  
535 for fieldwork assistance, and Western Michigan University for use of their facilities for this study.

## Data Availability

These data are being archived through PANGAEA (<https://www.pangaea.de/>).

## Author Contributions

KK wrote the manuscript, with feedback from all coauthors. KP designed the study, and SM and  
540 JE conducted the measurements and calibrations. KK led data analysis and interpretation, with  
contributions from SM, JE, QC, and KP. JDF assisted with the air turbulence measurements and analysis.  
SB coordinated logistics at the field site.

## Competing Interests

The authors declare that they have no conflict of interest.

## 545 References

Allan, B. J., Carslaw, N., Coe, H., Burgess, R. A. and Plane, J. M. C.: Observations of the nitrate radical  
in the marine boundary layer, *J. Atmos. Chem.*, 33(2), 129–154, doi:10.1023/A:1005917203307,



- 1999.
- Asaf, D., Tas, E., Pedersen, D., Peleg, M. and Luria, M.: Long-term measurements of NO<sub>3</sub> radical at a  
550 semiarid urban site: 2. Seasonal trends and loss mechanisms, *Environ. Sci. Technol.*, 44(15), 5901–  
5907, doi:10.1021/es100967z, 2010.
- Behnke, W., George, C., Scheer, V. and Zetzsch, C.: Production and decay of ClNO<sub>2</sub> from the reaction  
of gaseous N<sub>2</sub>O<sub>5</sub> with NaCl solution: Bulk and aerosol experiments, *J. Geophys. Res.*, 102, 3795–  
3804, doi:10.1029/96JD03057, 1997.
- 555 Bertram, T. H. and Thornton, J. A.: Toward a general parameterization of N<sub>2</sub>O<sub>5</sub> reactivity on aqueous  
particles: the competing effects of particle liquid water, nitrate and chloride, *Atmos. Chem. Phys.*, 9,  
8351–8363, doi:10.5194/acp-9-8351-2009, 2009.
- Brown, S. S., Dibb, J. E., Stark, H., Aldener, M., Vozella, M., Whitlow, S., Williams, E. J., Lerner, B.  
M., Jakoubek, R., Middlebrook, A. M., DeGouw, J. A., Warneke, C., Goldan, P. D., Kuster, W. C.,  
560 Angevine, W. M., Sueper, D. T., Quinn, P. K., Bates, T. S., Meagher, J. F., Fehsenfeld, F. C. and  
Ravishankara, A. R.: Nighttime removal of NO<sub>x</sub> in the summer marine boundary layer, *Geophys. Res.  
Lett.*, 31(7), 2–6, doi:10.1029/2004GL019412, 2004.
- Brown, S. S., Dubé, W. P., Tham, Y. J., Zha, Q., Xue, L., Poon, S., Wang, Z., Blake, D. R., Tsui, W.,  
Parrish, D. D. and Wang, T.: Nighttime chemistry at a high altitude site above Hong Kong, *J. Geophys.  
565 Res. Atmos.*, (3), 2457–2475, doi:10.1002/2015JD024566. Received, 2016.
- Chang, T. Y.: Rain and snow scavenging of HNO<sub>3</sub> vapor in the atmosphere, *Atmos. Environ.*, 18(1), 191–  
197, doi:10.1016/0004-6981(84)90242-7, 1984.
- Chang, W. L., Bhave, P. V., Brown, S. S., Riemer, N., Stutz, J. and Dabdub, D.: Heterogeneous  
Atmospheric Chemistry, Ambient Measurements, and Model Calculations of N<sub>2</sub>O<sub>5</sub>: A Review,  
570 *Aerosol Sci. Technol.*, 45(6), 665–695, doi:10.1080/02786826.2010.551672, 2011.
- Chen, Q., Edebeli, J., McNamara, S. M., Kulju, K. D., May, N. W., Bertman, S. B., Thanekar, S., Fuentes,  
J. D. and Pratt, K. A.: HONO, Particulate Nitrite, and Snow Nitrite at a Midlatitude Urban Site during  
Wintertime, *ACS Earth Sp. Chem.*, 3(5), 811–822, doi:10.1021/acsearthspacechem.9b00023, 2019.
- Christiansen, A., Carlton, A. and Henderson, B.: Differences in Fine Particle Chemical Composition on  
575 Clear and Cloudy Days, *Atmos. Chem. Phys.*, (March), 1–26, doi:10.5194/acp-2020-184, 2020.



- Crutzen, P. J.: The Role of NO and NO<sub>2</sub> in the Chemistry of the Troposphere and Stratosphere, *Ann. Rev. Earth Planet. Sci.*, 7, 443–72, doi:10.1146/annurev.ea.07.050179.002303, 1979.
- Dall’Osto, M., Harrison, R. M., Coe, H. and Williams, P.: Real-time secondary aerosol formation during a fog event in London, *Atmos. Chem. Phys.*, 9(7), 2459–2469, doi:10.5194/acp-9-2459-2009, 2009.
- 580 Fickert, S., Helleis, F., Adams, J. W., Moortgat, G. K. and Crowley, J. N.: Reactive uptake of ClNO<sub>2</sub> on aqueous bromide solutions, *J. Phys. Chem. A*, 102(52), 10689–10696, doi:10.1021/jp983004n, 1998.
- Finlayson-Pitts, B. J. . and Pitts, J. N. .: Formation of chemically active chlorine compounds by reactions of atmospheric NaCl particles with gaseous N<sub>2</sub>O<sub>5</sub> and ClONO<sub>2</sub>, *Nature*, 337(6204), 241–244, doi:10.1038/337241a0, 1989.
- 585 Ge, X., Zhang, Q., Sun, Y., Ruehl, C. R. and Setyan, A.: Effect of aqueous-phase processing on aerosol chemistry and size distributions in Fresno, California, during wintertime, *Environ. Chem.*, 9(3), 221–235, doi:10.1071/EN11168, 2012.
- Geyer, A., Alicke, B., Konrad, S., Schmitz, T., Stutz, J. and Platt, U.: Chemistry and oxidation capacity of the nitrate radical in the continental boundary layer near Berlin, *J. Geophys. Res. Atmos.*, 106(D8), 590 8013–8025, doi:10.1029/2000JD900681, 2001.
- Gržinić, G., Bartels-Rausch, T., Türler, A. and Ammann, M.: Efficient bulk mass accommodation and dissociation of N<sub>2</sub>O<sub>5</sub> in neutral aqueous aerosol, *Atmos. Chem. Phys.*, 17(10), 6493–6502, doi:10.5194/acp-17-6493-2017, 2017.
- Gunthe, S. S., Liu, P., Panda, U., Raj, S. S., Sharma, A., Darbyshire, E., Reyes-Villegas, E., Allan, J., 595 Chen, Y., Wang, X., Song, S., Pöhlker, M. L., Shi, L., Wang, Y., Kommula, S. M., Liu, T., Ravikrishna, R., McFiggans, G., Mickley, L. J., Martin, S. T., Pöschl, U., Andreae, M. O. and Coe, H.: Enhanced aerosol particle growth sustained by high continental chlorine emission in India, *Nat. Geosci.*, 14(2), 77–84, doi:10.1038/s41561-020-00677-x, 2021.
- Hahn, C. J.: A study of the diurnal behavior of boundary-layer winds at the Boulder Atmospheric 600 Observatory, *Boundary-Layer Meteorol.*, 21, 231–245, doi:10.1007/BF02033941, 1981.
- Heintz, F., Platt, U., Flentje, H. and Dubois, R.: Long-term observation of nitrate radicals at the Tor Station, Kap Arkona (Rügen), *J. Geophys. Res.*, 101(D17), 22891–22910, 1996.
- Huey, L. G., Tanner, D. J., Slusher, D. L., Dibb, J. E., Arimoto, R., Chen, G., Davis, D., Buhr, M. P.,



- Nowak, J. B., Mauldin, R. L., Eisele, F. L. and Kosciuch, E.: CIMS measurements of HNO<sub>3</sub> and SO<sub>2</sub>  
605 at the South Pole during ISCAT 2000, *Atmos. Environ.*, 38, 5411–5421,  
doi:10.1016/j.atmosenv.2004.04.037, 2004.
- Johnson, C. A., Sigg, L. and Zobrist, J.: Case studies on the chemical composition of fogwater: The  
influence of local gaseous emissions, *Atmos. Environ.*, 21(11), 2365–2374, doi:10.1016/0004-  
6981(87)90371-4, 1987.
- 610 Kercher, J. P., Riedel, T. P. and Thornton, J. A.: Chlorine activation by N<sub>2</sub>O<sub>5</sub>: simultaneous, in situ  
detection of ClNO<sub>2</sub> and N<sub>2</sub>O<sub>5</sub> by chemical ionization mass spectrometry, *Atmos. Meas. Tech.*, 2, 193–  
204, doi:10.5194/amt-2-193-2009, 2009.
- Leblanc, T. and Hauchecorne, A.: Recent observations of mesospheric temperature inversions, *J.*  
*Geophys. Res. Atmos.*, 102(D16), 19471–19482, doi:10.1029/97JD01445, 1997.
- 615 Liao, J., Sihler, H., Huey, L. G., Neuman, J. A., Tanner, D. J., Friess, U., Platt, U., Flocke, F. M., Orlando,  
J. J., Shepson, P. B., Beine, H. J., Weinheimer, A. J., Sjostedt, S. J., Nowak, J. B., Knapp, D. J.,  
Staebler, R. M., Zheng, W., Sander, R., Hall, S. R. and Ullmann, K.: A comparison of Arctic BrO  
measurements by chemical ionization mass spectrometry and long path-differential optical absorption  
spectroscopy, *J. Geophys. Res. Atmos.*, 116, 1–14, doi:10.1029/2010JD014788, 2011.
- 620 Lillis, D., Cruz, C. N., Collett, J., Willard Richards, L. and Pandis, S. N.: Production and removal of  
aerosol in a polluted fog layer: Model evaluation and fog effect on PM, *Atmos. Environ.*, 33(29),  
4797–4816, doi:10.1016/S1352-2310(99)00264-2, 1999.
- Lopez-Hilfiker, F. D., Constantin, K., Kercher, J. P. and Thornton, J. A.: Temperature dependent halogen  
activation by N<sub>2</sub>O<sub>5</sub> reactions on halide-doped ice surfaces, *Atmos. Chem. Phys.*, 12, 5237–5247,  
625 doi:10.5194/acp-12-5237-2012, 2012.
- Markovic, M. Z., Vandenboer, T. C. and Murphy, J. G.: Characterization and optimization of an online  
system for the simultaneous measurement of atmospheric water-soluble constituents in the gas and  
particle phases, *J. Environ. Monit.*, 14, 1872–1884, doi:10.1039/c2em00004k, 2012.
- McNamara, S. M., W. Raso, A. R., Wang, S., Thanekar, S., Boone, E. J., Kolesar, K. R., Peterson, P. K.,  
630 Simpson, W. R., Fuentes, J. D., Shepson, P. B. and Pratt, K. A.: Springtime Nitrogen Oxide-  
Influenced Chlorine Chemistry in the Coastal Arctic, *Environ. Sci. Technol.*, 53, 8057–8067,



- doi:10.1021/acs.est.9b01797, 2019.
- McNamara, S. M., Kolesar, K. R., Wang, S., Kirpes, R. M., May, N. W., Gunch, M. J., Cook, R. D.,  
Fuentes, J. D., Hornbrook, R. S., Apel, E. C., China, S., Laskin, A. and Pratt, K. A.: Observation of  
635 Road Salt Aerosol Driving Inland Wintertime Atmospheric Chlorine Chemistry, *ACS Cent. Sci.*, 5,  
doi:10.1021/acscentsci.9b00994, 2020.
- McNamara, S. M., Chen, Q., Edebeli, J., Kulju, K. D., Mumpfield, J., Fuentes, J. D., Bertman, S. B. and  
Pratt, K. A.: Observation of N<sub>2</sub>O<sub>5</sub> deposition and ClNO<sub>2</sub> production on the saline snowpack, *ACS  
Earth Sp. Chem.*, doi:10.1021/acsearthspacechem.0c00317, 2021.
- 640 Mielke, L. H., Furgeson, A. and Osthoff, H. D.: Observation of ClNO<sub>2</sub> in a Mid-Continental Urban  
Environment, *Environ. Sci. Technol.*, 45, 8889–8896, doi:10.1021/es201955u, 2011.
- Monin, A. S. and Obukhov, A. M.: Basic laws of turbulent mixing in the surface layer of the atmosphere.  
[online] Available from: [https://gibbs.science/teaching/efd/handouts/monin\\_obukhov\\_1954.pdf](https://gibbs.science/teaching/efd/handouts/monin_obukhov_1954.pdf)  
(Accessed 31 May 2019), 1954.
- 645 Neuman, J. A., Huey, L. G., Dissly, R. W., Fehsenfeld, F. C., Flocke, F., Holecek, J. C., Holloway, J. S.,  
Hübner, G., Jakoubek, R., Nicks, D. K., Parrish, D. D., Ryerson, T. B., Sueper, D. T. and Weinheimer,  
A. J.: Fast-response airborne in situ measurements of HNO<sub>3</sub> during the Texas 2000 Air Quality Study,  
*J. Geophys. Res. D Atmos.*, 107, 1–12, doi:10.1029/2001JD001437, 2002.
- Osthoff, H. D., Sommariva, R., Baynard, T., Pettersson, A., Williams, E. J., Lerner, B. M., Roberts, J.  
650 M., Stark, H., Goldan, P. D., Kuster, W. C., Bates, T. S., Coffman, D., Ravishankara, A. R. and Brown,  
S. S.: Observation of daytime N<sub>2</sub>O<sub>5</sub> in the marine boundary layer during New England Air Quality  
Study - Intercontinental Transport and Chemical Transformation 2004, *J. Geophys. Res. Atmos.*,  
111(23), 1–13, doi:10.1029/2006JD007593, 2006.
- Osthoff, H. D., Roberts, J. M., Ravishankara, A. R., Williams, E. J., Lerner, B. M., Sommariva, R., Bates,  
655 T. S., Coffman, D., Quinn, P. K., Dibb, J. E., Stark, H., Burkholder, J. B., Talukdar, R. K., Meagher,  
J., Fehsenfeld, F. C. and Brown, S. S.: High levels of nitryl chloride in the polluted subtropical marine  
boundary layer, *Nat. Geosci.*, 1, 324–328, doi:10.1038/ngeo177, 2008.
- Osthoff, H. D., Odame-ankrah, C. A., Tokarek, T. W., Taha, Y. M. and Corinne, L.: Low Levels of Nitryl  
Chloride in the Lower Fraser Valley of British Columbia, *Atmos. Chem. Phys.*, 18(2), 6293–6315,



- 660 2018.
- Phillips, G. J., Tang, M. J., Thieser, J., Brickwedde, B., Schuster, G., Bohn, B., Lelieveld, J. and Crowley, J. N.: Significant concentrations of nitryl chloride observed in rural continental Europe associated with the influence of sea salt chloride and anthropogenic emissions, *Geophys. Res. Lett.*, 39(10), 1–5, doi:10.1029/2012GL051912, 2012.
- 665 Pruppacher, H. R. and Klett, J. D.: *Microphysics of Clouds and Precipitation*, 2nd ed., 1997.
- Riedel, T. P., Wagner, N. L., Dubé, W. P., Middlebrook, A. M., Young, C. J., Öztürk, F., Bahreini, R., Vandenoer, T. C., Wolfe, D. E., Williams, E. J., Roberts, J. M., Brown, S. S. and Thornton, J. A.: Chlorine activation within urban or power plant plumes: Vertically resolved ClNO<sub>2</sub> and Cl<sub>2</sub> measurements from a tall tower in a polluted continental setting, *J. Geophys. Res. Atmos.*, 118, 8702–8715, doi:10.1002/jgrd.50637, 2013.
- 670 Roberts, J. M., Osthoff, H. D., Brown, S. S., Ravishankara, A. R., Coffman, D., Quinn, P. and Bates, T.: Laboratory studies of products of N<sub>2</sub>O<sub>5</sub> uptake on Cl<sup>-</sup> containing substrates, *Geophys. Res. Lett.*, 36(20), 1–5, doi:10.1029/2009GL040448, 2009.
- Sarwar, G., Simon, H., Xing, J. and Mathur, R.: Importance of tropospheric ClNO<sub>2</sub> chemistry across the Northern Hemisphere, *Geophys. Res. Lett.*, 41(11), 4050–4058, doi:10.1002/2014GL059962, 2014.
- 675 Seok, B., Helmig, D., Liptzin, D., Williams, M. W. and Vogel, C. S.: Snowpack-atmosphere gas exchanges of carbon dioxide, ozone, and nitrogen oxides at a hardwood forest site in northern Michigan, *Elementa*, 3, 1–20, doi:10.12952/journal.elementa.000040, 2015.
- Simpson, W. R., Brown, S. S., Saiz-Lopez, A., Thornton, J. A. and Von Glasow, R.: Tropospheric Halogen Chemistry: Sources, Cycling, and Impacts, *Chem. Rev.*, 115, 4035–4062, doi:10.1021/cr5006638, 2015.
- 680 Slusher, D. L., Huey, L. G., Tanner, D. J., Flocke, F. M. and Roberts, J. M.: A thermal dissociation - Chemical ionization mass spectrometry (TD-CIMS) technique for the simultaneous measurement of peroxyacyl nitrates and dinitrogen pentoxide, *J. Geophys. Res. Atmos.*, 109(19), 1–13, doi:10.1029/2004JD004670, 2004.
- Sommariva, R., Osthoff, H. D., Brown, S. S., Bates, T. S., Baynard, T., Coffman, D., De Gouw, J. A., Goldan, P. D., Kuster, W. C., Lerner, B. M., Stark, H., Warneke, C., Williams, E. J., Fehsenfeld, F.



- C., Ravishankara, A. R. and Trainer, M.: Radicals in the marine boundary layer during NEAQS 2004: A model study of day-time and night-time sources and sinks, *Atmos. Chem. Phys.*, 9(9), 3075–3093, doi:10.5194/acp-9-3075-2009, 2009.
- 690 Stanier, C., Singh, A., Adamski, W., Baek, J., Caughey, M., Carmichael, G., Edgerton, E., Kenski, D., Koerber, M., Oleson, J., Rohlf, T., Lee, S. R., Riemer, N., Shaw, S., Sousan, S. and Spak, S. N.: Overview of the LADCO winter nitrate study: Hourly ammonia, nitric acid and PM<sub>2.5</sub> composition at an urban and rural site pair during PM<sub>2.5</sub> episodes in the US Great Lakes region, *Atmos. Chem. Phys.*, 12(22), 11037–11056, doi:10.5194/acp-12-11037-2012, 2012.
- 695 Stull, R.: *Practical Meteorology: An Algebra-based Survey of Atmospheric Science.*, 1.02b., Univ. of British Columbia. [online] Available from: [https://www.eoas.ubc.ca/books/Practical\\_Meteorology/](https://www.eoas.ubc.ca/books/Practical_Meteorology/), 2017.
- Stull, R. B.: *An Introduction to Boundary Layer Meteorology.*, 1988.
- 700 Tham, Y. J., Wang, Z., Li, Q., Yun, H., Wang, W., Wang, X., Xue, L., Lu, K., Ma, N., Bohn, B., Li, X., Kecorius, S., Größ, J., Shao, M., Wiedensohler, A., Zhang, Y. and Wang, T.: Significant concentrations of nitryl chloride sustained in the morning: investigations of the causes and impacts on ozone production in a polluted region of northern China, *Atmos. Chem. Phys.*, 16, 14959–14977, doi:10.5194/acp-16-14959-2016, 2016.
- 705 Tham, Y. J., Wang, Z., Li, Q., Wang, W., Wang, X., Lu, K., Ma, N., Yan, C., Kecorius, S., Wiedensohler, A., Zhang, Y. and Wang, T.: Heterogeneous N<sub>2</sub>O<sub>5</sub> uptake coefficient and production yield of ClNO<sub>2</sub> in polluted northern China: Roles of aerosol water content and chemical composition, *Atmos. Chem. Phys.*, 18(17), 13155–13171, doi:10.5194/acp-18-13155-2018, 2018.
- Thornton, J. A. and Abbatt, J. P. D.: N<sub>2</sub>O<sub>5</sub> Reaction on Submicron Sea Salt Aerosol: Kinetics, Products, and the Effect of Surface Active Organics, *J. Phys. Chem. A*, 109, 10004–10012, doi:10.1021/jp054183t, 2005.
- 710 Thornton, J. A., Kercher, J. P., Riedel, T. P., Wagner, N. L., Cozic, J., Holloway, J. S., Dubé, W. P., Wolfe, G. M., Quinn, P. K., Middlebrook, A. M., Alexander, B. and Brown, S. S.: A large atomic chlorine source inferred from mid-continental reactive nitrogen chemistry, *Nature*, 464, 271–274, doi:10.1038/nature08905, 2010.
- 715





- 720 Wagner, N. L., Riedel, T. P., Young, C. J., Bahreini, R., Brock, C. A., Dubé, W. P., Kim, S., Middlebrook, A. M., Öztürk, F., Roberts, J. M., Russo, R., Sive, B., Swarthout, R., Thornton, J. A., VandenBoer, T. C., Zhou, Y. and Brown, S. S.:  $\text{N}_2\text{O}_5$  uptake coefficients and nocturnal  $\text{NO}_2$  removal rates determined from ambient wintertime measurements, *J. Geophys. Res. Atmos.*, 118, 9331–9350, doi:10.1002/jgrd.50653, 2013.
- Wang, S., Ackermann, R. and Stutz, J.: Vertical profiles of  $\text{O}_3$  and  $\text{NO}_x$  chemistry in the polluted nocturnal boundary layer in Phoenix, AZ: I. Field observations by long-path DOAS, *Atmos. Chem. Phys.*, 6(9), 2671–2693, doi:10.5194/acp-6-2671-2006, 2006.
- 725 Wang, S., McNamara, S. M., Kolesar, K. R., May, N. W., Fuentes, J. D., Cook, R. D., Gunsch, M. J., Mattson, C. N., Hornbrook, R. S., Apel, E. C. and Pratt, K. A.: Urban Snowpack  $\text{ClNO}_2$  Production and Fate: A One-Dimensional Modeling Study, *ACS Earth Sp. Chem.*, 4(7), 1140–1148, doi:10.1021/acsearthspacechem.0c00116, 2020.
- 730 Wang, X., Wang, H., Xue, L., Wang, T., Wang, L., Gu, R., Wang, W., Tham, Y. J., Wang, Z., Yang, L., Chen, J. and Wang, W.: Observations of  $\text{N}_2\text{O}_5$  and  $\text{ClNO}_2$  at a polluted urban surface site in North China: High  $\text{N}_2\text{O}_5$  uptake coefficients and low  $\text{ClNO}_2$  product yields, *Atmos. Environ.*, 156, 125–134, doi:10.1016/j.atmosenv.2017.02.035, 2017.
- Wood, E. C., Bertram, T. H., Wooldridge, P. J. and Cohen, R. C.: Measurements of  $\text{N}_2\text{O}_5$ ,  $\text{NO}_2$ , and  $\text{O}_3$  east of the San Francisco Bay, *Atmos. Chem. Phys.*, 4(5), 6645–6665, doi:10.5194/acp-5-483-2005, 2005.
- 735 Young, C. J., Washenfelder, R. A., Edwards, P. M., Parrish, D. D., Gilman, J. B., Kuster, W. C., Mielke, L. H., Osthoff, H. D., Tsai, C., Pikelnaya, O., Stutz, J., Veres, P. R., Roberts, J. M., Griffith, S., Dusanter, S., Stevens, P. S., Flynn, J., Grossberg, N., Lefer, B., Holloway, J. S., Peischl, J., Ryerson, T. B., Atlas, E. L., Blake, D. R. and Brown, S. S.: Chlorine as a primary radical: evaluation of methods to understand its role in initiation of oxidative cycles, *Atmos. Chem. Phys.*, 14, 3427–3440, doi:10.5194/acp-14-3427-2014, 2014.
- 740